Patterns in soil chemical weathering related to topographic gradients and vegetation structure in a high Andean tropical ecosystem

Armando Molina[1,2,3]; Veerle Vanacker[4], Marife Corre[2]; Edzo Veldkamp[2]

[1] Programa para el Manejo del Agua y del Suelo (PROMAS), Facultad de Ingeniería Civil, Universidad de Cuenca, Av. 12 de abril s/n, Cuenca, Ecuador.

[2] Soil Science of Tropical and Subtropical Ecosystems, Büsgen Institute, Georg-August-Universität Göttingen, Göttingen, Germany.

[3] Department of Earth and Environmental Sciences, KU Leuven, Celestijnenlaan 200E, 3001 Heverlee, Belgium.

[4] Earth and Life Institute, Georges Lemaitre Centre for Earth and Climate Research, University of Louvain, 3 Place Louis Pasteur, B-1348 Louvain-la-Neuve, Belgium.

Corresponding author: A. Molina (armando.molinav@ucuenca.edu.ec) and V. Vanacker (veerle.vanacker@uclouvain.be)

This article has been accepted for publication and undergone full peer review but has not been through the copyediting, typesetting, pagination and proofreading process which may lead to differences between this version and the Version of Record. Please cite this article as doi: 10.1029/2018JF004856

KEYPOINTS

- Spatial patterns in soil weathering extent are related to topographic gradients and vegetation patterns
- Mass losses of base cations and silica through chemical weathering facilitate downward migration and accumulation of organic constituents
- Rapid weathering of postglacial volcanic soils associated with accumulation of Al-humus complexes

ABSTRACT

Although climate exerts a major control on mineral weathering and soil formation processes, the combined effect of vegetation and topography can influence the rate and extent of chemical weathering at the hillslope scale. In this paper, we examined spatial patterns in volumetric strain and soil weathering extent associated with topographic gradients and vegetation patterns. In a high Andean catchment, we selected 10 soil toposequences on andesitic flows: 5 under tussock grasses, 3 under cushion forming plants and 2 under native forest. Along each toposequence, one pit was excavated at the shoulder, backslope and toeslope resulting in 30 soil profiles. Depth-weighted total soil porosity of the thirty soil profiles averaged 64±6%. The association between volumetric strain and soil organic C indicates that biotic agents can be effective in dilating the regolith during weathering. The young, postglacial volcanic soils were depleted in mono- and divalent cations, with total mass losses ranging between 793 and 1610 $kg.m^{-2}$. The accumulation of Al-humus complexes in the soil matrix plays an essential role in chemical transformation of the non-allophanic soils. Beyond the marginally significant topographic control on chemical weathering extent, our data show highly significant differences in chemical weathering extent between vegetation communities with total mass losses in forest soils being respectively 19% and 22% higher than in grasslands and cushion forming plants. The vegetation mosaic in alpine ecosystems might therefore provide essential clues to understand soil chemical weathering patterns caused by spatially varying soil particle and water residence times.

KEYWORDS

Chemical weathering, Soil development, Topographic control, Vegetation pattern, Páramo ecosystem, Soil toposequence, *Polylepis* forest, Cushion plants, High Tropical Andes, Andosol

1. INTRODUCTION

At the Earth's surface, mechanical disaggregation and chemical weathering transform bedrock into saprolite and soil. Hence, physical and chemical weathering processes fulfil a crucial function in the biogeochemistry of terrestrial ecosystems (Berner et al., 1983), and play an important role in many Earth surface processes (Ferrier & Kirchner, 2008). Rock-derived weathering products provide essential plant nutrients (Vitousek, 1995; see also Chadwick et al., 1999; Oh & Richter, 2005), and regulate the chemical composition of soil (Chadwick & Chorover, 2001; Riebe et al., 2004), surface and ground water (Markewitz et al., 2001, White et al., 2009). Chemical weathering facilitates mechanical disaggregation of rock into smaller fragments and physical erosion (Anderson et al., 2002; Schaller et al., 2010). Understanding the spatial variation of rock-derived weathering products across heterogeneous landscapes is important to constrain ecosystem processes.

The rate and extent of chemical weathering are influenced by the combined effects of climate, parent material, topography and vegetation (Jenny, 1941), and ultimately determine the mineral composition and element ratios of soil material (White et al., 2008). However, understanding the spatial and temporal variation of chemical weathering rates not only relies on knowledge of the environmental controls, but also of their interactions (Hartmann et al., 2014; Nezat et al., 2004, Schoonejans et al., 2016), whereas the relative importance of different controls may vary depending on the biogeochemical property of interest (Mage and Porder, 2013). Climate exerts a major control on chemical weathering and soil formation processes (Jenny, 1980; Rasmussen et al., 2011). Using climosequences along an altitudinal gradient in Hawaii, Chadwick et al. (2003) and Porder et al. (2007) showed that the weathering extent and soil properties are a nonlinear function of rainfall. They highlighted the

importance of effective soil moisture and soil physical properties in controlling water percolation, cation leaching, and soil formation (Chadwick et al., 2003).

Climate and parent material geochemistry can control soil nutrient content and water holding capacity (White et al., 1996), and by consequence vegetation patterns, as shown by e.g. Hahm et al. (2014) for the Sierra Nevada, California. In turn, vegetation has the potential to affect chemical weathering and soil formation (Amundson et al., 2015; Kelly et al., 1998; Lucas, 2001). Plants can influence the degree and rate of soil mineral weathering by enhancing physical and chemical weathering processes. Vegetation rooted in soil or weathered parent material can promote volume deformation (Merrits et al., 1992), physical disintegration (Viles, 1990) and bioturbation. For example, tree throw can homogenize topsoil and subsoil, and influence spatial patterns of soil horizon depths (Finke et al., 2013). Besides the effects on soil physical properties, plants can influence geochemical processes within the soil column as they produce CO_2, organic acids and ligands, which enhance chemical weathering by lowering pH and introducing organic chelates (Drever, 1994). Furthermore, by binding weathering products to soil organic matter components, they alter the exposed surface areas of the minerals and tend to extend the residence time of water in the soil system (Drever, 1994; Brantley et al., 2012). Furthermore, vegetation can alter soil hydrology, by changing the soil water balance and water movement in the soil system. The plant canopy intercepts rainfall by its leaves, stems and branches, plants control soil water losses through transpiration, and their roots and vacant macropores generally increase the soil's infiltration capacity and vertical preferential flow. Vegetation-driven change in water flow paths and rates in the soil system can have an effect on soil water residence time, and soil solute fluxes (Drever, 1994; see also Brantley et al., 2017; Kelly et al., 1998).

Researchers, studying the effect of slopes on weathering and pedogenesis, often use soil toposequences (catenas) to assess the effect of topography on the mobilization, redistribution and transfer of solutes, colloids, and particles along hillslopes (Khomo et al., 2011, 2013). Soil catenas typically reflect the transition from divergent, eroding areas to convergent, depositional areas, where losses or gains of dissolved and particulate soil constituents depend on topographic position (Bern et al., 2011). Studies using soil toposequences intend to isolate the topographic imprint on soil development and weathering (Chadwick & Asner, 2016; Schoonejans et al., 2017). However, interpretations are often difficult since local topography not only controls surface hydrology and redistribution of colloids and particles, it also affects soil nutrient status and vegetation development (Bailey et al., 2014; Tromp-van Meerveld & McDonnell, 2006).

In this study, we examined spatial patterns in volumetric strain and soil weathering extent across hillslopes, and their association with vegetation and topographic position. High Andean tropical ecosystems provide a good opportunity to study the association between chemical weathering, local topography and vegetation patterns: the climate, parent material and soil age can be held constant at the landscape scale, while the vegetation and slope morphology can vary greatly from the hilltops to the valley bottoms. The Andosols developed on volcanic parent material were exposed following deglaciation since the Last Glacial Maximum (Hansen et al., 2003). They are characterised by distinctive physicochemical and mineralogical properties due to their aluminium-rich elemental composition, large (reactive) specific surface areas, and high soil organic carbon stocks. In the 4.2 km² high Andean catchment, ten soil toposequences were sampled under three distinctive vegetation types to determine spatial patterns in soil weathering extent across the landscape. We assessed the extent of soil weathering using a geochemical mass balance that quantifies elemental losses

and gains and total mass losses, and the corresponding volumetric strain in soil and saprolite (Brimhall & Dietrich, 1987; Brimhall et al., 1992; Chadwick et al., 1990). In this study, we posit that the weathering extent of the soil mantle differs between (i) vegetation types and (ii) hillslope scale topographic positions.

2. PARAMO ECOSYSTEM

In the northern Andes, the alpine tundra or so-called páramo ecosystem encompasses a vegetation belt between the continuous forest line and the perpetual snow line, at elevations ranging from 3000 to 4500 m a.s.l. (Ramsay & Oxley, 1997; Sarmiento et al., 2003). In these high altitude ecosystems, the climate is generally cold and humid throughout the year accompanied with constant night frosts, intense solar radiation, and high relative humidity (Aparecido et al., 2017; Buytaert et al., 2011). Precipitation is highly variable and characterized by continuous moisture in the form of rain, clouds, and fog. The annual rainfall amount ranges from 500 to 3000 mm, and increases with altitude. Strong diurnal temperature fluctuations are common, ranging from below freezing to as high as 20° C (Aparecido et al., 2017). Soils are typically developed on volcanic rock and ash deposits: soils are dark in colour, low in pH, depleted in inorganic nutrients and have abundant organic carbon content in the uppermost horizons (Nierop et al., 2007; Ramsay & Oxley, 1997) . Grass páramo covers the largest area, and is composed of tussock grasses, cushion plants, thickets of small shrubs and patches of *Polylepis* forest (Sklenar & Ramsay, 2001).

2.1 Selection of study area

Our study area was located in the 4.2 km² Cuevas catchment on the western Cordillera in southern Ecuador (Figure 1), about 30 km southwest of the city of Cuenca (3°01’50” S, 79°17’59” W). Since 2010, the area is owned and protected by the public drinking water

company (ETAPA EP). Elevation ranges from 3608 to 3960 m a.s.l, with slopes of 5 to 12% in the flat valley bottoms, and hillslope gradients of 12 to 25%. The slope morphology was formed during the Pleistocene under the influence of glacial conditions, as shown by the presence of U-shaped valleys, glacial lakes and moraines (Jantz & Behling, 2012).

Climate is characterized by an udic moisture regime and an isomesic temperature regime (Buytaert et al., 2005a; Poulenard et al., 2003). Mean annual rainfall at the Soldados meteorological station (3500 m) is 911 mm for the period 1998 to 2013 (ETAPA EP), and exhibits a bimodal regime (Mora & Willems, 2012). February to April is the most humid period with a monthly precipitation of slightly more than 100 mm, while July and August is the dry season with a monthly precipitation of about 35 mm. In addition to the rainfall, there is continuous moisture input from clouds and fog in this high altitude páramo ecosystem (Molina et al., 2015). The mean annual air temperature is 8°C with little seasonal variation (ETAPA EP). However, large variations in air temperature occur between day and night, with maximum temperatures of 18 °C during the day and a minimum temperature of about 1°C during the night. Evapotranspiration is low due to low temperature and high air humidity, and the actual evapotranspiration is estimated to be 50 to 60% of the total annual rainfall (Carrillo-Rojas et al., 2019).

2.2 Volcanic soils and parent material

The formation and development of Andosols is conditioned by the geochemical properties of the volcanic material and the soil age (Buytaert et al., 2005b; Podwojewski & Poulenard, 2000). In central and northern Ecuador, vitric and allophanic Andosols are found near or within the active volcanic zones. Here, soils are continuously replenished with unweathered primary minerals because of high rates of volcanic ash input resulting in soils rich in

minerals. However, with increasing distance from the active volcanic zones, the thickness of distal tephras decreases rapidly. Our study area is located at the southernmost limit of recent volcanic ash deposits, and the effect of Holocene distal tephras on soil formation is thus limited (Rodbell et al., 2002, Figure 1). The soils developed on Mio-Pliocene andesitic parent material (Beate et al., 2001), that became exposed after the late Pleistocene glaciation (Hansen et al., 2003). Previous clay mineralogical studies suggested the prevalence of non-allophanic Andosols in southern Ecuador (Buytaert et al., 2005b; Podwojewski & Poulenard, 2000). In these non-allophanic Andosols, the topsoil is low in allophane and kaolin minerals while metal-humus complexes are abundant as result of the advanced stage of weathering. Soils are acidic with pH below 5, and typically have high water retention, low bulk density, and a loamy soil texture (Buytaert et al., 2005b; Poulenard et al., 2003).

2.3 Vegetation and land use

The grass páramo of the Cuevas catchment has a dense vegetation cover of 70 to 90% areal coverage. Tussock grasses are the dominant vegetation type (Figure 1), and they typically belong to bunch grasses of the *Stipa* and *Calamagrostis* genera of the Poaceae. Other abundant genera include Poaceae (*Paspalum and Cortaderia*), Hypericaceae *(Hypericum*), and Valerianaceae *(Valeriana*) (Jantz & Behling, 2012). Cushion forming plants mostly belonging to Plantaginaceae (*Plantago rígida*) and Cyperaceae (*Uncinia*) genera occur alongside the tussock grasses (Sklenár & Ramsay, 2001; White, 2013). Patches of *Polylepis* woodlands (*Polylepis reticulate)* are found in topographically protected sites in the upper parts of the catchment, and could be remnants of more extensive upper Andean forest in the past. The current mosaic of tussock grasses, cushion forming plants, and forest patches is not only the result of local climatic and topographic constraints (Jantz &Behling, 2012), but also of anthropogenic disturbances from human-induced fires and animal grazing (Ramsay, 1998;

Sklenar &Ramsay, 2001; White, 2013). Although the study area is part of a protected area since 2010, the study site is not devoid of human disturbance since the area was extensively grazed in the past. Burning of bunch grasses to facilitate reshooting of fresh sprouts continues to be practised in these traditional cattle-raising systems, although with less frequency and intensity than before (White, 2013).

3. MATERIALS AND METHODS

3.1 Soil and rock sampling

Within the 4.2 km² study site, we selected 10 soil toposequences (catenas) with similar slope gradient and curvature : 5 under tussock grasses (PR), 3 under cushion forming plants (CU), and 2 under native *Polylepis* forest (FR). Along each toposequence, one soil profile was excavated at the shoulder, backslope and toeslope position (Figure 1), resulting in a total of 30 soil profiles. Soil pits were excavated to a depth of more than 15 cm below the soil weathering front, reaching depths of 57 cm to 120 cm. We sampled and described the soil profiles based on genetic horizons following the procedures of the World Reference Base for Soil Resources (FAO, 2006). Undisturbed soil samples were taken per horizon with a soil core sampler for determination of the soil bulk density. We were unable to reach the bedrock in all pits, because of rising water entering the soil pit. In the pits where we could reach the bedrock, we sampled large rock fragments of the andesitic parent material and took representative pieces with a diameter of 5 to 10 cm. After removing the weathering rinds using a saw, we crushed the rock samples and prepared them for elemental analyses.

Because of the limited number of rock samples, we evaluated their representativeness by comparing their elemental composition with published data on the element abundances of andesite samples from nearby sites (Beate et al., 2001). The five rock samples described in Beate et al. (2001) (i.e., QC142, QC141, QC246, QC212, QC153) correspond to the same

lithological unit, and were sampled at <3 km distance from the 30 soil profiles. The location of the samples is shown in Figure 1. The bulk density of the parent material was derived from specific gravity measures of drill core samples that were realized by the IAMGOLD pre-feasibility study (Vallières et al., 2009) in the Quimsacocha area (about 1 km southeast of the study site).

3.2 Soil and rock chemical analyses

For determination of soil bulk density, the undisturbed soil core samples were dried at 105 °C during 24 h, and weighted. Disturbed soil samples taken from genetic horizons were air dried and passed through a 2 mm sieve to obtain the fine earth fraction for laboratory analyses. In most of the samples, the coarse soil fraction was below 5% and too low in lithic fragments to process them for geochemical analyses. A subsample of the air-dried soil was ground to powder using a ball mill for the determination of organic C and N. Total organic C and N were determined using CNS Elemental Analyzer (Elementar Vario EL, Hanau, Germany). Soil pH was measured from a saturated paste mixture using the soil:water (1:1 ratio of soil to H_2O) method. Effective cation exchange capacity (ECEC) was determined from soil samples percolated with unbuffered 1 mol L^{-1} NH_4Cl, and the percolates were analysed for exchangeable cations (Ca, Mg, K, Na, Al, Fe and Mn). The ECEC was calculated as the sum of the exchangeable base cations and exchange acidity. Dissolution analyses were conducted for the determination of poorly ordered materials. The Al_o was estimated by extraction with 0.2 M ammonium oxalate solution at pH 3 using a soil/solution ratio of 1:100 and shaking during 4 hours in the dark. Pyrophosphate extractions were used to estimate the aluminum associated with soil organic matter, Al_p. These extractions were conducted with a 0.1 M sodium pyrophosphate solution at pH 10, using a 1:100 soil/solution ratio and shaking samples for 16 hours in the dark. The solutions were analysed by inductively coupled plasma

emission spectrometry (iCAP 6300 Duo VIEW ICP Spectrometer, Thermo Fischer Scientific GmbH, Dreieich, Germany). The previously described analyses were conducted at the laboratory of the Soil Science of Tropical and Subtropical Ecosystems group of the University of Gottingen in Germany.

Total element analysis of the soil fine earth (< 2 mm) fraction and crushed rock samples was conducted at the Department of Earth and Environmental Sciences, KULeuven in Belgium. Soil and rock samples were powdered in a mortar grinder for about 8 minutes and were then placed in 5 ml tubes. 100 mg of the pulverized samples was mixed with 500 mg $LiBO_2$ (Lithium metaborate) in a graphite crucible and fused at 1000 °C for 10 minutes. The molten bead was then dissolved in a solution of 50 ml HNO_3 (0.42 M) on a magnetic stir plate. Solutions were measured with an ICP-AES (Inductively coupled plasma atomic emission spectroscopy) and analysed for Al, Fe, Ca, Mg, Na, K, Mn, P, Si, Ti and Zr. Loss on ignition (LOI) was determined following combustion of powdered aliquots in a muffle furnace at 1000 °C. We refer to Table S3 and S4 in the supplementary materials where the soil and rock elemental composition is presented on oxide basis (wt %). The elemental composition of the samples was corrected for blank, and is expressed in reference to the soil dry weight at 105°C (Table 2, S2, S4).

3.3 Quantifying physical deformation and chemical depletion

The intensity of weathering is here assessed as the fraction of mass lost by chemical weathering. We used a chemical mass balance approach where we evaluated the elemental mass losses or gains in soil compared to parent material using conservative element concentrations (Brimhall & Dietrich, 1987; Brimhall et al., 1992; Chadwick et al., 1990).

This approach builds upon the reliability of the conservative element for the normalization. In this study, we did not account for potential dust input nor made any correction for the soil coarse fraction. Coarse fragments were so low in abundance in the soil mantle (< 5% by volume), that their contribution to the calculation was negligible.

To assess the volumetric change of parent material when it is transformed to soil material, we calculated the physical deformation or volumetric strain, $\varepsilon_{i,w}$, from changes in bulk density of parent and weathered material following Brimhall and Dietrich (1987):

$$\varepsilon_{i,w} = \frac{(\rho_p C_{i,p})}{(\rho_w C_{i,w})} - 1$$

where ρ is the bulk density, C_i is the bulk concentration of an immobile element, and the subscripts *w* and *p* refer to weathered horizons and parent material, respectively (Brimhall & Dietrich, 1987; Brimhall et al., 1992; Chadwick et al., 1990). The bulk element concentrations were corrected for LOI (Table S4). Compaction of material results in $\varepsilon_{i,w} < 0$, while dilation results in $\varepsilon_{i,w} > 0$ (Brimhall et al., 1992). We used the median bulk density of the andesitic parent material, ρ_p, of 2.55 g/cm³ (n = 1038) as determined by Vallières et al. (2009) in our calculations.

We report the chemical mobility of individual elements within the weathered profile as mass transfer coefficients or tau, τ_j, values that describe the fractional mass gain ($\tau_{j,w} > 0$) or loss ($\tau_{j,w} < 0$) relative to the composition of the parent material (Brimhall & Dietrich, 1987):

$$\tau_{j,w} = \frac{\rho_w C_{j,w}}{\rho_p C_{j,p}} (\varepsilon_{i,w} + 1) - 1 = \frac{C_{j,w} C_{i,p}}{C_{j,p} C_{i,w}} - 1$$

where C_j is the bulk concentration of the element of interest, C_i the bulk concentration of the immobile element, and the subscripts *w* and *p* refer to weathered horizons and parent

material, respectively (Brimhall et al., 1992; Chadwick et al., 1990). Based on the comparison of Zr to Ti concentrations in parent material and soil samples (Figure S1), we decided to use Ti as the conservative element for the mass balance calculations. The Ti/Zr ratio of the soil samples deviates from the Ti/Zr enrichment line, indicating small losses of Zr relative to Ti. This is consistent with previous observations that have shown that Zr might become mobile in volcanic soils that develop in humid environments (Dixon et al., 2016; Kurtz et al., 2000; Little & Lee, 2006; Porder & Chadwick, 2009; Porder et al., 2007). Given that we cannot entirely exclude Ti mobility during intense weathering, we acknowledge that our mass losses are minimum estimates.

Finally, we assessed the total mass loss from chemical weathering, δ_{total}, per unit area (g cm^{-2}) for the entire weathering profile based on the mass transfer coefficients, $\tau_{j,w}$, using the approach proposed by Porder et al. (2007):

$$\delta_{total} = \sum_{h=1}^{n} \rho_p z_h \left(\sum_{j=1}^{m} \tau_{j,w} C_{j,p} \right)$$

where ρ_p is the bulk density of the parent material, Z_h the thickness of the h^{th} horizon, n the number of horizons in the weathering profile, $C_{j,p}$ the fraction of element j^{th} in the parent material, and m the number of chemical elements. In this method, the fraction of mass loss in each horizon is multiplied by the bulk density of the parent material to arrive at the chemical mass loss per genetic horizon. The mass loss per horizon is then weighted by its thickness and summed over all horizons in the weathering zone. To normalize soils to equivalent depths we either extended or reduced the thickness of the lowest horizon to reach 100 cm as normalized depth for the mass balance calculations following Chadwick et al. (2003) and Melzer et al. (2012). All mass losses were calculated on an oxide basis, and converted to kg m^{-2} (Table 3) to obtain the mass lost per unit area of the weathering profiles.

3.4 Multi-proxy approach to estimate chemical weathering intensity

To determine the reliability of the geochemical mass balance approach in our study sites, we compared the results on chemical depletion (obtained via the method described above) with estimates of the chemical index of alteration (CIA., Kirkwood & Nesbitt, 1991), the silicon-aluminium ratio (SA., Ruxton, 1968), and the total reserve in bases (TRB., Herbillon, 1986). The latter three weathering indices were applied in the past to measure the extent of saprolite and soil weathering by e.g. Burke et al. (2007, 2009) and Ameijeiras-Mariño et al. (2017). These indices are also based on the major and minor element chemistry of soil and rock samples, but they do not incorporate mass balance principles. Hence, they provide a relative measure of the degree of weathering that is dependent on bedrock mineralogy. We refer to the older work cited above for a detailed description of the chemical weathering indices.

It is not our purpose to provide an extensive comparison of soil weathering indices, but rather to validate the geochemical mass balance approach through a comparative analysis with three different measures of weathering degree. As the total mass loss (kg m^{-2}), the chemical index of alteration, the silicon-aluminium ratio and the total reserve in bases are indicators of the extent of chemical weathering, we plotted them against soil pH to analyze systematic variation in chemical weathering degree and chemical depletion.

3.5 Statistical Analysis

We tested whether the soil physico-chemical properties and degree of chemical weathering are different (1) in soils covered with *polylepis* forest, tussock grasses and cushion forming plants and (2) in soils on shoulder, back slope and toeslope positions. All comparisons were realized on the depth-weighted averages per soil profiles. A sketch of the statistical design is given in the supplementary materials (Figure S2).

The comparisons of the weathering extent between the three vegetation types (FR, CU, PR), and between the hillslope-scale topographic positions (upper, middle and lower) across vegetation types were performed using one-way analysis of variance. Because of limited accessibility to forest sites, the number of soil profiles is not equal for the three vegetation groups, with 6 soil profiles in *Polylepsis* forest, 9 in cushion forming plants and 15 in tussock grasses. We first tested for homogeneity of variance and normality using the Shapiro-Wilk test ($p < 0.05$). When the assumptions of homogeneity of variance and normality were met, the group comparison was done with one-way ANOVA, followed by the Holm-Sidak posthoc test for multiple comparisons. When one of the two criteria were not met, the Kruskas-Wallis ANOVA on the ranks was applied, with the Dunn's posthoc test. We rejected the null hypotheses (i.e. that there are no differences between the means of the three groups) at the 0.05 significance level.

4. RESULTS

First, we characterised the volcanic soils that develop in high alpine páramo environments based on the analysis of their morphological and physico-chemical properties, and volumetric strain. After validating the chemical mass balance approach through a comparative analysis of weathering indices, we then analysed the chemical depletion of the soils based on their elemental and total mass losses. Finally, we assessed the association of the depth-weighted soil properties and chemical weathering extent with topographic gradient and vegetation type. A summary of the one-way analyses of variance is given in Table 4.

4.1 Soil morphology and physicochemical composition

Independent of topography and vegetation types, soils had similar morphological and diagnostic properties. Soil profiles were generally thin since the depth to the C horizon ranged from 27 to 100 cm, with the thinnest soil profiles in the area covered by cushion plants (Table 1). The soils displayed distinctive horizons with contrasting colour and structure: the uppermost organic matter rich horizons of mobile regolith were characterized by a very dark colour (10 YR 1.7/1) with granular and crumb structure (A horizons). The A horizons were abruptly separated from, and in sharp contrast to the underlying AC, CA and C horizon that exhibited light coloured (e. g. brownish or yellowish) subsoil or saprolite material that lacked structure. For further analyses, the weathering profiles were partitioned into two "layers" with the upper organic matter rich A horizons named "soil" and the lower horizons "saprolite".

Organic carbon content in the weathering profiles ranged from 0.10 to 21%, with an average of 4.5±2.5%, and was significantly greater in the A horizons (9.4±4.2%) compared to the AC, CA or C horizons (Table S2). Dry bulk density was on average 1.0 ± 0.3 g cm^{-3} and varied from 0.28 to 1.4 g cm^{-3} with the lowest values of 0.70±0.21 g cm^{-3} observed in the A horizons. Soil organic carbon is negatively correlated with dry bulk density (Spearman correlation coefficient, $r = -0.73$, $n = 95$, p-value < 0.01). The combination of high organic carbon content (> 3%) and dry bulk density (< 0.9 g cm^{-3}) in the A horizons indicated that the soils met the diagnostic criteria for Andosols according to the WRB classification (Table 1). Along the soil catenas, we did not detect significant differences in organic carbon content and bulk density between vegetation types or topographic positions (Table 4).

The pH in the weathering profile ranged from 4.2 to 6.4, with an average of 5.1±0.4 (Table S2). The pH of the soil generally increased with depth with the A horizons being more acidic (4.9 ± 0.4) than the saprolitic subsoil (5.4±0.5). Unlike organic carbon and bulk density, we observe highly significant differences in soil pH between vegetation types (Table 4). The most acidic soils were observed in forests and páramo grasslands with average pH values of respectively 4.8 and 5.0, significantly lower than the average soil pH values of 5.6 observed in areas covered by cushion plants (Table 1). The Al_p in the soil profile varied from 0.2 to 25.8 g kg^{-1}, with an average of 5.4±4.8 g kg^{-1}, whereas the Al_o ranged from 3.1 to 31.8 g kg^{-1}, with an average of 8.9±4.9 g kg^{-1} (Table S2). Both Al_p and Al_o decrease with depth, with above average values in the organic-rich A horizons (8.0±4.8 g kg^{-1} and 11.2±5.2 g kg^{-1}, respectively), pointing to the presence of Al-humus complexes.

4.2. Volumetric strain

All soil profiles have undergone similar volumetric expansion and collapse, with strain values being high and positive in the upper organic horizons that have undergone expansion relative to the parent material, and strain values being close to zero in the saprolite (Figure 2, Table S2). Marked differences exist in volumetric strain within the weathering profiles, Figure 3 shows that the volumetric changes are positively related to soil organic C content. The relationship between the amount of dilation and organic C content is highly significant for soil horizons with a carbon content above 3% (Spearman correlation coefficient = 0.86, p-value < 0.01). Organic-rich A horizons underwent a volumetric expansion of 230±160 % on average when converted into soil material, with dilation values up to 550 % (Table S4). In contrast, the underlying AC, CA and C horizons underwent minor dilation of respectively 60±40%, 40±30% and 50±56% on average (Table S4). No statistically significant differences

in volumetric strain were observed between topographic positions or vegetation types (Table 4).

4.3. Multi-proxy evaluation of the chemical weathering extent

Table 3 reports four indices of chemical weathering: the chemical index of alteration (CIA), total reserve in bases (TRB) and silicon-aluminium (SA) ratio and total mass loss (TML). Similar to our measures of strain and mass transfer coefficients, the total mass loss estimates derived from the geochemical mass balance can be subject to underestimation due to an incomplete retention of Ti in the soil system. Figure 4 shows the four weathering indices as a function of the soil pH. There is a positive and significant relationship between the soil pH and total mass loss (Spearman r =0.56, p-value < 0.01), TRB (r=0.60, p-value < 0.01), SA (0.49, p-value < 0.01) and CIA (-0.69, p-value <0.01), pointing to an overall congruence in the dataset. This is further confirmed by the consistent results of the two one-way ANOVAs (Table 4).

4.4. Elemental transfers and total mass losses

The rock fragments of the andesitic parent material had SiO_2 as the most abundant oxide (62±2.1% by weight), followed by Al_2O_3 (18±0.9% by weight). Oxides of Ca and Na occurred at concentration levels of 4.8±0.1 and 4.4±0.3 wt% respectively (Table 2). The four rock samples were uniform in their elemental chemistry with relative differences in major elements concentrations of < 5% for Si, < 2 % for Al, and < 1.5 % for Ca, Na, K, Mg, and Fe. Minor constituents such as P and Mn show a relative difference of less than 0.04% and the trace constituents Ti and Zr display differences of 0.2 and 0.003% respectively. The elemental chemistry of major and trace (Ti) elements in our rock samples (Table 2) is statistically similar to the five rock samples of the same lithological unit (i.e. andesitic lava

flow of QVC phase 1) that were analysed by Beate et al. (2001, Table S3). From Figure 5, it can be seen that the major element chemistry of bedrock samples is highly uniform over the study area, compared to the observed differences with the soil chemistry. The minor variation in bedrock Ti concentrations shown in Table 2 is trivial compared to the variation between parent material and soil samples. As such, we used the average Ti concentration of the four rock samples in the mass balance calculations (Table 2).

Mass transfer coefficients indicated that the soils experienced intense weathering with significant elemental depletion throughout the soil profile (see Figure 6 for depth distribution of elemental mass transfer coefficients for all soil profiles, and Table 3 for depth-weighted elemental transfers per profile). Relative to Ti, the base cations displayed mean mass losses of 94±5 % for Ca, 94±5% for Na, 90±8% for K and 86±6% for Mg (Table 3). Depletion profiles did not show a clear trend in base cation losses with depth (Figure 6), and had rather uniform depletion of Ca, Na, K and Mg throughout all horizons. Silicon showed an average net loss of 54±6%, with only slight variations with depth (Figure 6), indicative for the high degree of chemical weathering. Al and Fe displayed lower mobility within the soil profiles, with a tau-value for Al of -0.12±0.11 and for Fe of -0.26±0.19. The element specific weathering extent varies by roughly 5 to 25% between soil profiles.

Our data show only marginally significant ($p < 0.10$) trends with hillslope-scale topographic positions (Table 4): the K, Mg, Na and Si cations were slightly less depleted in soils at the upper slope positions compared to the mid-slope and lower slope (Figure 7). The increase in mass loss along slope is less marked for the trivalent Al and Fe cations (Figure 8). In contrast, the difference in relative elemental losses between vegetation groups is statistically significant ($p < 0.05$) for the base cations (Table 4), with significantly higher losses of Ca, K

and Na in soils formed under forests and native grasslands compared to cushion plants. The metal cations show a slightly different pattern, with significantly higher fractional mass losses of Si and Fe in forests compared to native grasslands and cushion plants (Figure 8).

Total weight losses by chemical weathering for the 30 profiles ranged between 793 and 1610 kg m^{-2}, with a mean value of 1240±210 kg m^{-2} (Table 3). Almost 70% of the total chemical mass loss was due to the loss of Si. The relative order of the elemental mass losses was Si > (Ca, Na) > Al > (Fe, Mg) > K, with the highest coefficients of variation observed for Al and Fe weight losses. Total weight losses by chemical weathering show only marginally significant ($p < 0.10$) differences along slope (Table 4), with the total mass losses increasing with increasing distance from the crest (Figure 9). Total mass losses are significantly different ($p < 0.05$) between vegetation types, with soil columns in native forest having chemical mass losses of 1440±130 kg m^{-2}, respectively 19% (1210 kg m^{-2}) and 22% (1170 kg m^{-2}) higher than the mass losses in tussock grasses and cushion forming plants (Table 3). The Si and Fe balance in the forest soils is strongly negative, with average elemental mass losses of Si and Fe of respectively 956±86 and 70±7 kg m^{-2}. Soils covered by cushion forming plants have the lowest mass loss (1170±190 kg m^{-2}), and are significantly less depleted in calcium, sodium and potassium (Figure 7). The mobilisation of Si and Fe is reduced in cushion soils, with elemental mass losses of respectively 799±123 and 24±14 kg m^{-2}. Soils covered by tussock grasses have intermediate levels of mass losses, of 1210±200 kg m^{-2}. They are strongly depleted in base cations similar to the forest soils, but show a large range in Si and Fe losses that are statistically not discernible from forest and cushion soils (Table 4).

5. DISCUSSION

5.1. Creating porosity during Andosol development

Chemical transformation and physical deformation of soil material influence bulk density and porosity during soil development (Brimhall et al., 1992), and are essential for horizon differentiation in weathering profiles (Anderson et al., 2002). Our dataset provides relevant information for exploring the chemical, physical and biological processes responsible for the creation of pore space during Andosol formation. Depth-weighted total soil porosity of the 30 soil profiles averages 64±6%, and values up to 81% were measured similar to earlier observations by Poulenard et al. (2003). The variation in soil porosity and volumetric strain is largest in the upper 50 cm of the weathering profiles (Figure 2), and organic-rich horizons (with organic C content > 3%) experienced stronger dilation than organic-poor horizons (with organic C content ≤ 3%; Figure 3). In contrast to the depth dependence of volumetric strain, the mass transfer coefficients of the major elements do not show a clear variation with depth (Figure 6). These observations suggest that the physical deformation of the topsoil is rather associated with biological activity than mineral weathering or translocation. Positive volumetric strain in topsoil is not unusual, and is commonly attributed to organic matter accumulation (Brimhall et al., 1992; Chadwick et al., 1990; Oh and Richter, 2005) and/or physical increase in void space from bioturbation (Anderson et al., 2002). However, to our knowledge, few studies have reported positive strain values above 200%. We pose that during the early stages of Andosol formation, the pore and void space created by chemical weathering processes becomes rapidly colonized by the rhizosphere. Soil faunal bioturbation then further enhances the vertical distribution of soil organic matter over short vertical distances as shown by Tonneijck & Jongmans (2008), and likely plays an important role during physical deformation of the soil mantle. The formation of the porous topsoil can create preferential pathways for the movement of water and solutes (Navarrete-Sitchler et al., 2009).

The interaction of chemical transformation, physical deformation and biological processes can explain the intense weathering extent with strong depletion of monovalent and divalent cations throughout the soil profiles (Figure 6). The strong depletion of Ca and Na in the exchangeable pools (not shown) and the total pool from the parent material (τ_{Ca}= τ_{Na} = -0.94±0.08, Table 3) is coincident with the acidic soil conditions (pH = 5.2±0.4) and accumulation of exchangeable aluminium. Soil acidity is enhanced by chemical weathering, as the base cations Ca, Na and K are depleted by hydrolysis and solution reactions and the concentration of hydrogen ions (H^+) in the soil increases. We observed remarkably high concentrations of exchangeable Al in the páramo soils, with Al^{3+} being 56±31% of the effective cation exchange capacity (Table 1). While the udic moisture regime over the páramo ecosystem is favourable for intense leaching and soil weathering as suggested by Dixon et al. (2016) and Slessarev et al. (2016), there is reason to expect that biogeochemical processes driven by plants and soil microorganisms also enhance cation mobilization and soil acidification (Fujii et al., 2018; Reich et al., 2005). The accumulation of organic compounds in the pore space of the A horizons (as shown in Figure 3) typically leads to a release of carbonic and organic acids and changes the chemical composition of the soil pore water (Takahashi and Dahlgren, 2016). In the non-allophanic soils of our study area, aluminium-humus complexes (pyrophosphate-ectractable Al) form 49±16% of the active Al (oxalate-extractable Al), pointing to the importance of Al^{3+} complexation with organic substances through ligand exchange and hydrogen bonding (Mizota & van Reeuwijk, 1989; Kramer and Chadwick, 2016). Based on the highly significant correlation between Al-humus complex' content, organic C content (p-value<0.01), and total mass losses (p-value <0.05), we suggest that the Al-humus complexes play an essential role in chemical transformation of non-allophanic Andosols.

5.2. Chemical weathering along topographic gradients

A change in weathering intensity along topographic transects can be associated with (1) physical transport of weathered material downslope and/or (2) hillslope hydrology controlling spatial patterns in soil and subsoil water fluxes. Lateral redistribution of soil particles along slope can lead to an overall increase in soil residence time and degree of weathering downslope (Green et al., 2006; Yoo et al., 2009): when eroded soil particles are transported downslope, they can be reincorporated in the soil matrix and continue to weather chemically (Wackett et al., 2018). Along the 10 toposequences, we observed no differences in soil depth, volumetric deformation or soil acidity and only marginally significant differences in base cation mass transfer coefficients (Table 4). Soil particle transport by surface water runoff is likely to be slow in preserved páramo ecosystems, as shown by Poulenard et al. (2001) and Tenorio et al. (2018) for the nearby Tomebamba and Yanuncay catchments. The dense vegetation cover, high overall porosity (64±6 %) and soil organic C content (4.5±2.5 %, Table 1) of the páramo soils are favourable for soil infiltration, and inhibit surface runoff and detachment of soil particles by water. Saturation excess overland flow is only rarely observed in swales affected by overgrazing and fires (Iñiguez et al., 2016). The dominance of rounded hilltops suggests that diffusive processes such as bioturbation and soil creep play a major role in soil-landscape development in páramo ecosystems (Tonneijck & Jongmans, 2008; Vanacker et al., 2015). Slow diffusive transport of soil particles along slope may explain the minimal variation in soil physical properties that we observed along slope, and indicates a rather small effect of soil particle redistribution on the weathering extent of the soil material.

Besides lateral variation in soil particle redistribution along slope, soil and subsoil water fluxes also exhibit spatial variation in headwater basins. At the hillslope scale, soil water residence time and subsurface soil water flux commonly increase downslope (Asano et al.,

2002; McGuire et al., 2005). Longer fluid residence times facilitate chemical weathering and can lead to enhanced in-situ weathering rates (Maher, 2010, 2011). Currently, crucial data on the water balance, soil water and solute fluxes in páramo soils are lacking to quantify the impact of hillslope hydrology on in-situ soil weathering rates.

5.3. Chemical weathering and vegetation type

Soil chemical weathering is strongly coupled to the vegetation types ($p<0.05$, Table 4). The largest differences in weathering degree are observed between forests and cushion plants, with significantly higher Ca, K, Na, Si and Fe mass transfer coefficients, higher soil acidity, higher mobility of Al^{3+}, and larger total mass losses in forest soils compared to soils colonized by cushion plants (Table 4). Figure 4 illustrates that soils covered by forests and cushion forming plants form two distinct clusters in the (pH-weathering index) scatterplots. Soils covered by tussock grasses have a more mixed behaviour, and belong to one of the two above-mentioned groups depending on the weathering index under consideration.

Vegetation development can be conditioned by rock-derived soil nutrient supply and soil hydrology (Hahm et al., 2014), but in its turn vegetation can adapt itself by modifying the soil physico-chemical properties and soil water balance (Amundson et al., 2007; Fujii et al., 2018; Kelly et al., 1998). Enhanced cation leaching by carbonic and organic acids released by the dense and fine root' network in forests (Reich et al., 2005) can play a role in the stronger acidification and lower pool of base cations in forest soils compared to soils covered by cushion plants (Figure 9). The formation of Al-humus complexes further enhances the mobility of metal cations, whose solubility is typically low in abiological systems (Lucas, 2001). Although the significantly higher levels of exchangeable Al^{3+} that we measured in forest and grassland soils compared to the cushion plants (Table 4) could point to plant-

induced weathering processes, there are field-based indications that other factors related to subsurface hydrology might also play a role. Vegetation patterns and soil hydrological regime co-vary at the hillslope scale, as cushion plants, unlike forest and tussock grasses, frequently colonise moist microsites that are subject to saturation or waterlogging in the wettest periods of the year. Buytaert et al. (2006) reported seasonal waterlogging and low redox potential in páramo microsites with flow convergence, and the hydric soil properties provide morphological evidence of prolonged saturation in the soils covered by cushion plants. Under saturated conditions, the plant root growth and leaf area expansion are inhibited because of oxygen deficiency. In addition to the potential plant-induced effect of soil pH on mineral weathering, the hydric soil properties point to micro-sites where the convergence of flow paths and/or locally reduced soil hydraulic conductivity result in relatively long soil water residence times compared to forest or grassland sites. Whether the chemical weathering rate will steadily increase along slope or asymptote to a maximum solute flux at toeslope positions will critically depend on the water flow rate and the distance along slope where the soil water reaches chemical equilibrium (Maher, 2011). The soil solutes in sites characterised by relatively long subsurface flow paths due to within-hillslope convergence and/or low water flow rates tend to approach chemical equilibrium following Maher (2011), thereby limiting the potential for in-situ chemical weathering. As such, vegetation and soil weathering extent can co-vary at the hillslope scale, as result of spatially variable soil hydraulic conductivity and/or topographically controlled convergence or divergence of flow paths along slope.

6. CONCLUSIONS

Soils in páramo ecosystems of southern Ecuador are primarily non-allophanic Andosols developed on volcanic parent material. The young, postglacial soils experienced intense

weathering with strong depletion of the Ca, Na, and K base cations throughout the soil depth and total weight losses ranging between 793 and 1610 kg m^{-2}. The relative order of the elemental mass losses was Si > (Ca, Na) > Al > (Fe, Mg) > K, with almost 70% of the total chemical mass loss due to the loss of Si. The highest coefficients of variation were observed for Al and Fe weight losses. Páramo soils exhibit extraordinary characteristics for organic carbon accumulation and storage due to their unique physicochemical properties. Our data reveal that the organic horizons have soil bulk densities as low as 0.28 g cm^{-3}, and an organic carbon content up to 21%. During the early transformation of andesite to soil material, the matrix of the weathered bedrock is differentiated by chemical weathering. Pore space that is generated by a loss of mobile constituents through weathering reactions facilitates downward migration of organic constituents. The loss of the mobile constituents (base cations and Si) results in soils that are nearly devoid of primary minerals and become dominated by metal-humus complexes. The accumulation of metal-humus complexes plays an essential role in carbon storage, physical deformation and weathering of the non-allophanic Andosols.

The spatial pattern in soil biogeochemical properties reflects the association between soil chemical weathering, soil hydrology, physical transport of soil particles along slope, and vegetation distribution. A marginally significant increase in base cation depletion is observed along topographic gradients that can be associated with physical transport of weathered soil particles downslope or subsurface water fluxes. Beyond the hillslope-scale topographic control on chemical weathering extent, we observed highly significant differences in chemical weathering extent between vegetation communities with total mass losses in forest soils being respectively 19% and 22% higher than in grasslands and cushion forming plants. Although biotic factors can play a role in creating the observed patterns in soil development, the vegetation communities can also hint to the existence of hillslope micro-topography and

subsurface hydrological patterns that are very challenging to map in the field. The patchwork mosaic of tussock grasses, cushion plants and *Polylepis* forests in páramo ecosystems, might therefore provide essential clues to understand soil chemical weathering patterns in alpine ecosystems caused by spatially varying soil particle and soil water residence times.

ACKNOWLEDGEMENTS

This research was supported by the Alexander von Humboldt Foundation through a Georg Forster Fellowship for Postdoctoral Researchers (3.2-ECU/1138588 STP), and a Prometeo grant to AM funded by the Secretaría de Educación Superior, Ciencia, Tecnología e Innovación de la República del Ecuador. Fieldwork in Ecuador was facilitated through a collaborative research project between the Universidad de Cuenca, Université catholique de Louvain, Université de Namur, CGPaute (now SENAGUA) and ETAPA EP (Empresa Pública Municipal de Telecomunicaciones, Agua Potable, Alcantarillado y Saneamiento de Cuenca) funded by ARES (Academie de Recherche et Enseignement Supérieur de la Fédération Wallonie-Bruxelles, Belgium). We are thankful to Santiago Zhiminaicela and Juan Barahona who provided technical assistance including sample collection, and acknowledge Felipe Cisneros for continued support of our research activities in the High Andean headwater basins. The insightful and constructive reviews from three anonymous reviewers and the associated editor have stimulated us to sharpen our ideas, and they contributed greatly to improve our scientific contribution.

The data used are listed in the tables and supplements.

7. References

Ameijeiras-Mariño, Y., Opfergelt, S., Schoonejans, J., Vanacker, V., Sonnet, P., de Jong, J., & Delmelle, P. (2017). Impact of low denudation rates on soil chemical weathering intensity: a multiproxy approach. *Chemical Geology, 456,* 72–84.

Amundson, R., Heimsath, A. M., Owen, J. J., Yoo, K., & Dietrich, W. E. (2015). Hillslope soils and vegetation. *Geomorphology, 234,* 122–132.

Amundson, R., Richter, D.D., Humphreys, G.S., Jobbagy, E.G., & Gaillardet, J. (2007). Coupling between biota and earth materials in the critical zone. *Elements, 3*, 327-332.

Anderson, S.P., Dietrich, W.E., & Brimhall, G.H. (2002). Weathering profiles, mass-balance analysis, and rates of solute loss: linkages between weathering and erosion in a small, steep catchment. *Geological Society of America Bulletin, 114,* 1143–1158.

Aparecido L.M.T., Teodoro, G.S., Mosquera, G., Brum, M., de V. Barros, F., Vieira Pompeu, P., et al. (2018). Ecohydrological drivers of Neotropical vegetation in montane ecosystems. *Ecohydrology. e1932.*

Asano, Y., Uchida, T., & Ohte, N. (2002). Residence times and flow paths of water in steep unchannelled catchments, Tanakami, Japan. *Journal of Hydrology, 261,* 173– 192.

Bailey, S.W., Brousseau, P.A., McGuire, K.J., & Ross, D.S. (2014). Influence of landscape position and transient water table on soil development and carbon distribution in a steep, headwater catchment. *Geoderma, 226,* 279-289.

Beate, B., Monzier, M., Spikings, R., Cotton, J., Silva, J., Bourdon, E., & Eissen, J.P. (2001). Mio-Pliocene adakite generation related to flat subduction in southern Ecuador: the Quimsacocha volcanic center. *Earth and Planetary Science Letters, 192,* 561-570.

Bern, C.R., Chadwick, O.A., Hartshorn, A.S., Khomo, L.M., & Chorover, J. (2011). A mass-balance model to separate and quantify colloidal and solute redistributions in soil. *Chemical Geology, 282,* 113-119.

Berner, R.A., Lasaga, A.C., & Garrels, R.M. (1983). The carbonate silicate geochemical cycle and its effect on atmospheric carbon dioxide over the past 100 million years. *American Journal of Science, 283,* 641–683.

Brantley, S.L., & Chen, Y. (1995). Chemical weathering rates of pyroxenes and amphiboles. In A.F.White & S.L. Brantley (Eds.), *Chemical Weathering Rates of Silicate Minerals*, (pp. 119–172), Washington, D.C: Mineralogical Society of America.

Brantley, S.L., Eissenstat, D.M., Marshall, J.A., Godsey, S.E., Balogh-Brunstad, Z.B., Karwan, D.L., et al. (2017). Reviews and syntheses: on the roles trees play in building and plumbing the critical zone. *Biogeosciences*, *14*, 5115-5142.

Brantley, S.L., Lebedeva, M., & Hausrath, E.M. (2012). A geobiological view of weathering and erosion. In A. Knoll (Eds.), *Fundamentals of Geobiology*, (pp. 205-227), West Sussex, UK: Wiley-Blackwell.

Brimhall, G.H., Chadwick, O.A., Lewis, C.J., Compston, W., Williams, I.S., Danti, K.J., et al. (1992). Deformational mass transport and invasive processes in soil evolution: *Science, 255*(5045), 695–702.

Brimhall, G.H., & Dietrich, W.E. (1987). Constitutive mass balance relations between chemical composition, volume, density, porosity, and strain in metasomatic hydrochemical systems: Results on weathering and pedogenesis. *Geochimica et Cosmochimica Acta*, *51*(3), 567–587.

Burke, B.C., Heimsath, A.M., Dixon, J.L., Chappell, J., & Yoo, K. (2009). Weathering the escarpment: Chemical and physical rates and processes, south-eastern Australia. *Earth Surface Processes and Landforms*, *34*, 768–785.

Burke, B.C., Heimsath, A.M., & White, A.F. (2007). Coupling chemical weathering with soil production across soil-mantled hillslopes. *Earth Surface Processes and Landforms, 32*, 853–873.

Buytaert, W., Cuesta-Camacho, F., & Tobon, C. (2011). Potential impacts of climate change on the environmental services of humid tropical alpine regions. *Global Ecology and Biogeography*, *20(1)*, 19–33.

Buytaert, W., De Bièvre, B., Wyseure, G., & Deckers, J. (2005a). The effect of land use changes on the hydrological behaviour of Histic Andosols in south Ecuador. *Hydrological Processes, 19,* 3985–3997.

Buytaert, W., Deckers, J., & Wyseure, G. (2006). Description and classification on nonallophanic Andosols in south Ecuadorian alpine grasslands (paramo). *Geomorphology, 73*, 207-221.

Buytaert, W., Sevink, J., De Leeuw, B., & Deckers, J. (2005b). Clay mineralogy of the soils in the south Ecuadorian páramo region. *Geoderma, 127,* 114–129.

Chadwick, O.A., Brimhall, G H., & Hendricks, D.M. (1990). From a black to a gray box-A mass balance interpretation of pedogenesis. *Geomorphology, 3*(3–4), 369–390.

Chadwick, O.A., & Chorover, J. (2001). The chemistry of pedogenic thresholds. *Geoderma, 100*(3–4), 321–353.

Chadwick, O.A., Derry, L.A., Vitousek, P.M., Huebert, B.J., & Hedin, L.O. (1999). Changing sources of nutrients during four million years of ecosystem development. *Nature, 397*(6719), 491–497.

Chadwick, O.A., Gavenda, R.T., Kelly, E.F., Ziegler, K., Olson, C.G., Elliott, W.C., & Hendricks, D.M. (2003). The impact of climate on the biogeochemical functioning of volcanic soils. *Chemical Geology, 202,* 195–223.

Chadwick, K.D., & Asner, G.P. (2016) Tropical soil nutrient distributions determined by biotic and hillslope processes. *Biogeochemistry, 127*(2-3), 273-289.

Dixon, J.L., Chadwick, O.A., & Vitousek, P.M. (2016). Climate-driven thresholds for chemical weathering in postglacial soils of New Zealand. *Journal of Geophysical Research: Earth Surface, 121,* 1619–1634.

Drever, J.I. (1994). The effect of land plants on weathering rates of silicate minerals. *Geochimica et Cosmochimica Acta, 58,* 2325–2332.

FAO, (2006). *World reference base for soil resources 2006. A framework for international classification, correlation and communication.* Rome: World Soil Resources Reports No 103, FAO/ISRIC/IUSS.

Ferrier, K.L., & Kirchner, J.W. (2008). Effects of physical erosion on chemical denudation rates: A numerical modeling study of soil-mantled hillslopes. *Earth and Planetary Science Letters, 272*(3–4), 591–599.

Finke, P.A., Vanwalleghem, T., Opolot, E., Poesen, J., & Deckers, J. (2013). Estimating the effect of tree uprooting on variation of soil horizon depth by confronting pedogenetic simulations to measurements in a Belgian loess area. *Journal of Geophysical Research: Earth Surface, 118*, 2124–2139.

Green, E.G., Dietrich, W.E., & Banfield, J.F. (2006) Quantification of chemical weathering rates across an actively eroding hillslope. *Earth and Planetary Science Letters, 242*, 155-169.

Hahm, W.J., Riebe, C.S., Lukens, C.E., & Araki, S. (2014). Bedrock composition regulates mountain ecosystems and landscape evolution. *Proceedings of the National Academy of Sciences of the United States of America, 111*(9), 3338–3343.

Hansen, B.C.S, Rodbell, D.T., Seltzer, G.O., Leon, B., Young, K.R., & Abbott, M. (2003). Late-glacial and Holocene vegetational history from two sites in the western Cordillera of southwestern Ecuador. *Palaeogeography, Palaeoclimatology, Palaeoecology, 194*, 79-108.

Hartmann, J., Moosdorf, N., Lauerwald, R., Hinderer, M., & West, A.J. (2014). Global chemical weathering and associated P-release. The role of lithology, temperature and soil properties. *Chemical Geology, 363*, 145–163.

Herbillon, A.J. (1986). Chemical estimation of weatherable minerals present in the diagnostic horizons of low activity clay soils. In F.H. Beinroth et al. (Eds.), *Proceedings of 8th International Soil Classification Workshop: Classification, Characterization and Utilization of Oxisols* (pp. 39-48). Rio de Janeiro: EMBRAPA.

Iñiguez, V., Morales, O., Cisneros, F., Bauwens, W., & Wyseure, G. (2016). Analysis of the drought recovery of Andosols on southern Ecuadorian Andean páramos. *Hydrology and Earth System Sciences, 20*, 2421-2435.

Jantz, N., & Behling, H. (2012). A Holocene environmental record reflecting vegetation, climate, and fire variability at the Páramo of Quimsacocha, southwestern Ecuadorian Andes. *Vegetation History and Archaeobotany, 21*, 169–185.

Jenny, H. (1941). Factors of soil formation. New York: McGraw-Hill.

Jenny, H. (1980). The Soil Resource: Origin and Behavior. New York: Spring Verlag.

Kelly, E.F., Chadwick, O.A., & Hilinski, T.E. (1998). The effects of plants on mineral weathering. *Biogeochemistry, 42*, 21–53.

Khomo, L., Bern, C.R., Hartshorn, A.S., Rogers, K.H., & Chadwick, O.A. (2013). Chemical transfers along slowly eroding catenas developed on granitic cratons in southern Africa. *Geoderma, 202–203*, 192–202.

Khomo, L., Hartshorn, A.S., Rogers, K.H., & Chadwick, O.A. (2011). Impact of rainfall and topography on the distribution of clays and major cations in granitic catenas of southern Africa. *Catena, 87,* 119–128.

Kirkwood, D.E., & Nesbitt, H.W. (1991). Formation and evolution of soils from an acidified watershed, Plastic Lake, Ontario, Canada. *Geochimica et Cosmochimica Acta, 55,* 1295–1308.

Kramer, M.G. & O.A. Chadwick (2016). Controls on carbon storage and weathering in volcanic soils across a high-elevation climate gradient on Mauna Kea, Hawaii. *Ecology 97(9),* 2384-2395.

Kurtz, A.C., Derry, L.A., Chadwick, O.A., & Alfano, M. J. (2000). Refractory element mobility in volcanic soils. *Geology, 28,* 683–686.

Little, M.G., Lee, C.-T.A. (2006). On the formation of an inverted weathering profile on Mount Kilimanjaro, Tanzania: Buried paleosol or groundwater weathering? *Chemical Geology, 235*(3-4), 205-221.

Lucas, Y. (2001). The role of plants in controlling rates and products of weathering: importance of biological pumping. *Annual Review of Earth and Planetary Sciences, 29,* 135–163.

Mage, S., & Porder, S. (2013). Parent material and topography determine soil phosphorus status in the Luquillo Mountains of Puerto Rico. *Ecosystems, 16,* 284–294.

Maher, K. (2010). The dependence of chemical weathering rates on fluid residence time. *Earth and Planetary Science Letters, 294*(1-2), 101-110.

Maher, K. (2011). The role of fluid residence time and topographic scales in determining chemical fluxes from landscapes. *Earth and Planetary Science Letters, 312*(1–2), 48–58.

Markewitz, D., Davidson, E.A., Figueiredo, R.D.O., Victoria, R.L., & Krusche, A.V. (2001). Control of cation concentrations in stream waters by surface soil processes in an Amazonian watershed. *Nature, 410,* 802–805.

McGuire, K.J., McDonnell, J.J., Weiler, M., Kendall, C., McGlynn, B.L., Welker, J.M., & Seibert, J. (2005). The role of topography on catchment-scale water residence time. *Water Resources Research, 41,* W05002.

Melzer, S.E., Chadwick, O.A., Hartshorn, A.S., Khomo, L. M., Knapp, A.K., & Kelly, E.F. (2012). Lithologic controls on biogenic silica cycling in South African savanna ecosystems. *Biogeochemistry, 108,* 317 –334.

Merritts, D.J., Chadwick O.A., Hendricks D.M., Brimhall G.H., & Lewis C.J. (1992). The mass balance of soil evolution on late Quaternary marine terraces, northern California. *Geological Society of America Bulletin, 104,* 1456–1470.

Mizota, C., & Van Reeuwijk, L.P. (1989). Clay mineralogy and chemistry of soils formed in volcanic material in diverse climatic regions. *Soil Monographs*. (Vol. 2). Wageningen: ISRIC.

Molina, A., Vanacker, V., Brisson, E., Mora, D., & Balthazar, V. (2015). Multidecadal change in streamflow associated with anthropogenic disturbances in the tropical Andes. *Hydrology and Earth System Sciences, 19,* 4201–4213.

Mora, D.E., & Willems, P. (2012). Decadal oscillations in rainfall and air temperature in the Paute River Basin-Southern Andes of Ecuador. *Theoretical and Applied Climatology, 108,* 267–282.

Navarre-Sitchler, A., Steefel, C.I., Yang, L., Tomutsa, L., & Brantley, S.L. (2009). Evolution of porosity and diffusivity associated with chemical weathering of a basalt clast. *Journal of Geophysical Research: Earth Surface, 114*, F02016.

Nezat, C.A., Blum, J.D., Klaue, A., Johnson, C.E., & Siccama, T.G. (2004). Influence of landscape position and vegetation on long-term weathering rates at Hubbard Brook Experimental Forest, New Hampshire, USA. *Geochimica et Cosmochimica Acta, 68*, 3065–3078.

Nierop, K.G.J., Tonneijck, F.H., Jansen, B., & Verstraten, J.M. (2007). Organic matter in volcanic ash soils under forest and páramo along an Ecuadorian altitudinal transect. *Soil Science Society of America Journal, 71*, 1119–1127.

Oh, N.-H., & Richter, D.D. (2005). Elemental translocations and loss from three highly weathered soil-bedrock profiles in the southeastern United States. *Geoderma, 126*, 5–25.

Podwojewski, P., & Poulenard, J. (2000). Los suelos del páramo del Ecuador. *Serie Páramo*. (Vol. 5). Quito: GTP/ Abya Yala.

Porder, S., & Chadwick, O.A. (2009). Climate and soil-age constraints on nutrient uplift and retention by plants. *Ecology, 90*(3), 623-636.

Porder, S., Hilley, G.E., & Chadwick, O.A. (2007). Chemical weathering, mass loss, and dust inputs across a climate by time matrix in the Hawaiian Islands. *Earth and Planetary Science Letters, 258*(3-4), 414–427.

Poulenard, J., Podwojewski, P., & Herbillon, A.J. (2003). Characteristics of non-allophanic Andisols with hydric properties from the Ecuadorian páramos. *Geoderma, 117*, 267– 281.

Poulenard, J., Podwojewski, P., Janeau, J.L., & Collinet, J. (2001). Runoff and soil erosion under rainfall simulation of Andisols from the Ecuadorian paramo: Effect of tillage and burning. *Catena, 45*, 185–207.

Ramsay, P.M., & Oxley, E.R.B. (1997) The growth form composition of plant communities in the Ecuadorian paramos. *Plant ecology, 131*, 173-192.

Rasmussen, C., Brantley, S., Richter, D.D., Blum, A., Dixon, J., & White, A.F. (2011). Strong climate and tectonic control on plagioclase weathering in granitic terrain. *Earth and Planetary Science Letters, 301*(3–4), 521–530.

Reich, P.B., Oleksyn, J., Modrzynski, J., Mrozinski, P., Hobbie, S.E., Eissenstat, D.M., Chorover, J., Chadwick, O.A., Hale, C.M., & Tjoelker, M.G (2005). Linking litter calcium, earthworms and soil properties: a common garden test with 14 tree species. *Ecology letters, 8(8),* 811-818.

Riebe, C.S., Kirchner, J.W., & Finkel, R.C. (2004). Sharp decrease in long-term chemical weathering rates along an altitudinal transect. *Earth and Planetary Science Letters, 218*, 421–434.

Rodbell, D.T., Bagnato, S., Nebolini, J.C., Seltzer, G.O., & Abbott, M.B. (2002). A Late-Glacial–Holocene tephrochronology for glacial lakes in southern Ecuador. *Quaternary Research, 57,* 343–354.

Ruxton, B.P. (1968). Measures of the degree of chemical weathering of rocks. *Journal of Geology, 76*, 518–527.

Sarmiento, L., Llambí, L.D., Escalona, A., & Marquez, N. (2003). Vegetation patterns, regeneration rates and divergence in an old-field succession of the high tropical Andes. *Plant Ecology*, *166*(1), 145–156.

Schaller, M., Blum, J.D., Hamburg, S.P., & Vadeboncoeur, M.A. (2010). Spatial variability of long-term chemical weathering rates in the White Mountains, New Hampshire, USA. *Geoderma, 154*, 294–301.

Schoonejans, J., Vanacker, V., Opfergelt, S., Ameijeiras-Mariño, Y., & Christl, M. (2016). Kinetically limited weathering at low denudation rates in semiarid climatic conditions. *Journal of Geophysical Research: Earth Surface, 121*(2), 336–350.

Schoonejans, J., Vanacker, V., Opfergelt, S., & Christl, M. (2017). Long-term soil erosion derived from in-situ ^{10}Be and inventories of meteoric ^{10}Be in deeply weathered soils in southern Brazil. *Chemical Geology*, *466,* 380-388.

Sklenár P., & Ramsay, P.M. (2001) Diversity of zonal paramo plant communities in Ecuador. *Diversity and Distributions*, *7*(3), 113-124.

Slessarev, E.W., Lin, Y., Bingham, N.L., Johnson, J.E., Dai, Y., Schimel, J.P., & Chadwick, O.A. (2016). Water balance creates a threshold in soil pH at the global scale. *Nature, 540*, 567-569.

Takahasi, T., & Dahlgren, R.A. (2016). Nature, properties and function of aluminium-humus complexes in volcanic soils. *Catena, 263*, 110-121.

Tenorio, G.E., Vanacker, V., Campforts, B., Álvarez, L., Zhiminaicela, S., Vercruysse, K., Molina, A., & Govers, G. (2018). Tracking spatial variation in river load from Andean highlands to inter-Andean valleys. *Geomorphology, 308*, 175-189.

Tonneijck, F. H., & Jongmans, A. G. (2008). The influence of bioturbation on the vertical distribution of soil organic matter in volcanic ash soils: a case study in northern Ecuador. *European Journal of Soil Science, 59*, 1063–1075.

Tromp-van Meerveld, H.J., & McDonnell, J.J. (2006). On the interrelations between topography, soil depth, soil moisture, transpiration rates and species distribution at the hillslope scale. *Advances in Water Resources, 29*(2), 293–310.

Vallières, D., Pelletier, P., & Clouston, F. (2009). *Technical report on the Quimsacocha Gold project, Azuay Province, Ecuador*. (NI-43-101 Technical Report). Québec, Canada: IAMGOLD Technical Services.

Vanacker, V., von Blanckenburg, F., Govers, G., Molina, A., Campforts, B., & Kubik, P.W. (2015). Transient river response, captured by channel steepness and its concavity. *Geomorphology, 228*, 234-243.

Viles, H.A. (1990). The agency of organic beings: a selective review of recent work in biogeomorphology. In J.B. Thornes (Ed.), *Vegetation and erosion: processes and environments*, (pp. 5-25). Chichester: Wiley.

Vitousek, P.M. (1995). The Hawaiian Islands as a model system for ecosystem studies, *Pacific Science, 49*(1), 2–16.

Wackett, A.A., Yoo, K., Amundson, R., Heimsath, A.M., & Jelinski, N.A. (2018). Climate controls on coupled processes of chemical weathering, bioturbation, and sediment transport across hillslopes. *Earth Surface Processes and Landforms*, *43*, 1575-1590.

White, A.F., Blum, A.E., Schulz, M.S., Bullen, T.D., Harden, J.W., & Peterson, M.L. (1996). Chemical weathering rates of a soil chronosequence on granitic alluvium: I. Quantification of mineralogical and surface area changes and calculation of primary silicate reaction rates. *Geochimica et Cosmochimica Acta, 60,* 2533–2550.

White, A.F., Schulz, M.S., Stonestrom, D.A., Vivit, D.V., Fitzpatrick, J., Bullen, T.D., Maher, K., & Blum, A.E. (2009). Chemical weathering of a marine terrace chronosequence, Santa Cruz, California Part II: Solute profiles, gradients and the comparisons of contemporary and long-term weathering rates. *Geochimica et Cosmochimica Acta, 73*(10), 2769–2803.

White, A.F., Schulz, M.S., Vivit, D.V., Blum, A.E., Stonestrom, D.A., & Anderson, S.P. (2008). Chemical weathering of a marine terrace chronosequence, Santa Cruz, California I: Interpreting rates and controls based on soil concentration-depth profiles. *Geochimica et Cosmochimica Acta, 72,* 36–68.

White, S. (2013). Grass páramo as hunter-gatherer landscape. The Holocene 23(6): 898-915.

Yoo, K., Mudd, S.M., Sanderman, J., Amundson, R., & Blum, A. (2009). Spatial patterns and controls of soil chemical weathering rates along a transient hillslope. *Earth and Planetary Science Letters, 288*(1-2), 184-193.

Table 1. Physical and chemical properties of the 30 soil profiles. The data are shown as depth-weighted averages (100 cm), and are rounded to two significant digits. The soil profiles are coded as following: the first two letters of the profile ID refer to the vegetation type, with FR=*Polylepis* forest, PR= tussock grasses and CU= cushion forming plants. This is followed by a number referring to the replicate soil toposequence (1 to 5), and the topographic position of the soil pit along the slope with Upper = shoulder or "upper slope", Middle = backslope or "mid-slope" and Lower = toeslope or "lower slope" position.

Profile	Vegetation	pH	Al^{3+}	ECEC	BS	BD	OC	Al_p	Al_o	SD
		-	cmol(+) kg^{-1}	cmol(+) kg^{-1}	%	g cm^{-3}	%	g kg^{-1}	g kg^{-1}	cm
FR2 Upper	Forest	5.2	3.4	6.9	45	1.1	3.1	3.0	9.1	50
FR2 Middle	Forest	5.1	5.9	8.7	38	1.1	4.3	3.9	7.9	55
FR2 Lower	Forest	5.0	4.5	6.8	33	0.82	8.3	5.7	8.4	93
FR3 Upper	Forest	4.5	7.8	9.5	12	0.97	6.6	7.5	10.4	60
FR3 Middle	Forest	4.6	4.1	4.9	13	1.1	2.2	4.0	9.0	45
FR3 Lower	Forest	4.5	5.6	7.0	16	0.86	4.5	11.7	17.0	65
PR1 Upper	Grass	5.2	3.5	8.4	62	0.76	3.5	2.8	7.0	27
PR1 Middle	Grass	5.0	5.4	7.0	20	0.99	2.1	2.2	4.8	66
PR1 Lower	Grass	5.1	4.4	6.6	32	1.2	1.6	1.7	3.9	54
PR2 Upper	Grass	5.0	6.5	7.3	8	0.92	4.7	9.2	14.7	85
PR2 Middle	Grass	4.8	6.8	8.5	14	1.00	3.7	6.1	9.4	100
PR2 Lower	Grass	5.2	5.6	7.7	34	0.86	3.9	4.6	9.0	75
PR3 Upper	Grass	5.2	8.5	10	22	0.50	12	12.6	13.7	65
PR3 Middle	Grass	4.9	9.9	11	11	0.90	8.1	9.7	14.1	60
PR3 Lower	Grass	5.1	4.9	6.3	24	1.0	3.8	3.0	5.9	45
PR4 Upper	Grass	5.0	6.5	7.2	8	1.0	6.5	6.6	10.3	55
PR4 Middle	Grass	5.0	9.4	11	9	0.76	9.1	8.5	12.1	95
PR4 Lower	Grass	5.0	10	11	7	0.77	7.4	12.3	12.9	80
PR5 Upper	Grass	5.2	5.5	11	49	1.0	2.7	4.2	6.6	62
PR5 Middle	Grass	5.0	8.3	13	32	1.0	4.0	7.1	8.5	57
PR5 Lower	Grass	4.9	6.4	11	41	1.1	4.1	3.8	6.8	52
CU2 Upper	Cushion	6.0	0.73	15	97	0.76	5.1	3.2	7.6	35
CU2 Middle	Cushion	5.3	3.0	7.1	55	0.81	3.9	2.4	8.5	40
CU2 Lower	Cushion	5.3	3.1	7.1	59	0.89	4.0	3.5	7.3	40
CU3 Upper	Cushion	5.6	0.45	7.5	93	1.0	3.2	0.9	4.5	37
CU3 Middle	Cushion	5.8	0.36	7.7	95	0.92	2.3	1.4	5.3	57
CU3 Lower	Cushion	5.7	0.40	6.6	93	1.0	2.2	3.2	7.8	43
CU4 Upper	Cushion	5.9	0.19	12	98	1.1	1.5	2.5	3.6	43
CU4 Middle	Cushion	5.6	0.71	15	94	1.2	2.6	1.2	4.5	42
CU4 Lower	Cushion	5.4	1.0	10	90	1.1	3.0	3.4	5.1	41
Mean ± 1 SD										
FR	Forest	4.8±0.3	5.2±1.6	7.3±1.6	26±14	0.99±0.13	4.8±2.3	6.0±3.2	10.3±3.4	61±17
PR	Grass	5.0±0.1	6.8±2.0	9.1±2.1	25±17	0.92±0.17	5.1±2.3	6.3±3.5	9.3±3.5	65±19
CU	Cushion	5.6±0.3	1.1±1.1	9.8±3.4	86±17	0.98±0.14	3.1±2.9	2.4±1.0	6.0±1.8	42±6
ALL		5.2±0.4	4.8±3.0	9.0±2.6	44±32	0.95±0.15	4.5±2.5	5.1±3.4	8.5±3.4	58±19

Al^{3+} = Exchangeable aluminum, ECEC = Effective cation exchange capacity, calculated as the sum of exchangeable base and acidic cations, BS = Base saturation, calculated as the total reserve in bases (Ca, K, Mg, Na) divided by the ECEC, BD = Bulk density, OC = Organic carbon content, Al_p = Pyrophosphate-extractable aluminum, Al_o = Oxalate-extractable aluminum and SD = Soil depth to C horizon.

Table 2. Chemical composition of parent material. The elemental chemistry is presented on oxide basis (wt %) for the major elements, and in element concentration (mg/kg) for Zr. The elemental data is presented as bulk values, and the reported values are corrected for loss on ignition and rounded to two significant digits.

	CaO	K_2O	MgO	Na_2O	Al_2O_3	Fe_2O_3	SiO_2	TiO_2	Zr
	%	%	%	%	%	%	%	%	ppm
PR2 Upper	4.8	1.2	1.6	4.5	17	5.3	63	0.80	130
PR3 Middle	4.7	1.2	2.6	4.1	19	5.6	59	0.93	150
FR3 Upper	4.8	1.4	1.7	4.5	17	4.3	63	0.69	160
CU3 Middle	4.9	1.4	1.5	4.7	18	4.4	64	0.74	160
Mean ± 1 SD									
this study	4.8±0.1	1.3±0.1	1.9±0.5	4.4±0.3	18±0.9	4.9±0.7	62±2.1	0.79±0.10	150±13
Beate et al. (2001)	5.3±0.3	1.4±0.1	1.6±0.2	4.6±0.2	18±0.2	4.8±0.4	62±0.6	0.73±0.05	110±3

Table 3. Mass transfer coefficients (τ), total mass losses, volumetric strain, and the chemical weathering indices expressed as depth-weighted averages (100 cm). Values are rounded to two significant digits, with exception of the TML values that are rounded to three significant digits.

Profile	τ Ca	τ K	τ Mg	τ Na	τ Al	τ Fe	τ Si	TML kg m^{-2}	Strain	CIA	SA	TRB $cmol_c$ kg^{-1}
FR2 Upper	-0.96	-0.92	-0.85	-0.97	-0.11	-0.45	-0.53	-1240	0.54	99	1.9	42
FR2 Middle	-0.98	-0.96	-0.93	-0.98	-0.17	-0.56	-0.60	-1410	0.66	99	1.7	22
FR2 Lower	-0.97	-0.94	-0.92	-0.98	-0.20	-0.58	-0.58	-1390	1.9	99	1.9	22
FR3 Upper	-0.98	-0.96	-0.93	-0.98	-0.23	-0.57	-0.61	-1450	0.90	99	1.8	23
FR3 Middle	-0.99	-0.97	-0.94	-0.99	-0.28	-0.59	-0.69	-1610	0.20	99	1.6	23
FR3 Lower	-0.96	-0.96	-0.88	-0.97	-0.25	-0.63	-0.64	-1520	0.66	99	1.7	40
PR1 Upper	-0.91	-0.82	-0.82	-0.90	0.21	0.10	-0.40	-809	1.9	98	1.7	62
PR1 Middle	-0.99	-0.97	-0.93	-0.98	0.068	0.18	-0.51	-1060	0.78	100	1.6	18
PR1 Lower	-0.98	-0.97	-0.93	-0.98	0.038	0.094	-0.51	-1090	0.46	99	1.7	21
PR2 Upper	-0.98	-0.97	-0.90	-0.98	-0.14	-0.28	-0.63	-1400	0.98	99	1.5	29
PR2 Middle	-0.97	-0.98	-0.89	-0.98	-0.084	-0.28	-0.60	-1340	0.29	99	1.5	27
PR2 Lower	-0.95	-0.93	-0.83	-0.96	-0.065	-0.39	-0.55	-1260	1.3	98	1.7	47
PR3 Upper	-0.87	-0.70	-0.60	-0.86	0.078	0.60	-0.42	-793	NA	96	1.9	59
PR3 Middle	-0.98	-0.96	-0.92	-0.98	-0.22	-0.53	-0.63	-1480	1.7	99	1.7	20
PR3 Lower	-0.99	-0.95	-0.94	-0.98	-0.11	-0.52	-0.56	-1320	1.1	100	1.7	18
PR4 Upper	-0.99	-0.97	-0.94	-0.99	-0.089	-0.51	-0.57	-1320	1.2	100	1.7	14
PR4 Middle	-0.98	-0.96	-0.91	-0.98	-0.10	-0.32	-0.55	-1270	3.0	99	1.8	16
PR4 Lower	-0.98	-0.93	-0.92	-0.98	-0.080	-0.35	-0.54	-1240	2.6	99	1.8	18
PR5 Upper	-0.95	-0.77	-0.65	-0.91	-0.18	-0.10	-0.51	-1190	0.93	97	2.1	82
PR5 Middle	-0.97	-0.87	-0.85	-0.96	-0.060	-0.25	-0.48	-1120	1.0	99	1.9	36
PR5 Lower	-0.97	-0.88	-0.87	-0.96	-0.33	-0.24	-0.58	-1400	0.63	98	2.2	43
CU2 Upper	-0.92	-0.96	-0.87	-0.97	-0.035	0.030	-0.49	-1090	2.6	98	1.9	30
CU2 Middle	-0.89	-0.95	-0.68	-0.95	-0.10	-0.19	-0.58	-1270	1.6	97	1.6	79
CU2 Lower	-0.96	-0.95	-0.92	-0.97	0.20	-0.29	-0.44	-950	2.1	99	1.6	20
CU3 Upper	-0.63	-0.72	-0.80	-0.65	-0.14	-0.29	-0.42	-979	1.0	87	2.4	180
CU3 Middle	-0.91	-0.87	-0.88	-0.92	-0.22	-0.03	-0.56	-1230	1.0	96	2.1	67
CU3 Lower	-0.91	-0.82	-0.89	-0.90	-0.21	-0.21	-0.52	-1230	0.72	96	2.2	70
CU4 Upper	-0.77	-0.67	-0.77	-0.71	-0.14	-0.26	-0.39	-953	0.90	89	2.6	140
CU4 Middle	-0.85	-0.76	-0.88	-0.84	-0.37	-0.25	-0.51	-1270	0.41	91	2.9	110
CU4 Lower	-0.93	-0.85	-0.88	-0.93	-0.45	-0.26	-0.63	-1520	0.88	96	2.3	73
Mean (1 SD)												
Forest (FR)	-0.97	-0.95	-0.91	-0,98	-0,21	-0,56	-0,61	-1440	0,81	99	1,8	29
	(0.01)	*(0.02)*	*(0.04)*	*(0,01)*	*(0,06)*	*(0,06)*	*(0,05)*	*(130)*	*(0,58)*	*(0)*	*(0,1)*	*(10)*
Grass (PR)	-0.96	-0.91	-0.86	-0,96	-0,07	-0,19	-0,54	-1210	1,3	99	1,8	34
	(0.03)	*(0.08)*	*(0.10)*	*(0,04)*	*(0,13)*	*(0,13)*	*(0,07)*	*(200)*	*(0,8)*	*(1)*	*(0,2)*	*(21)*
Cushion (CU)	-0.86	-0.84	-0.84	-0,87	-0,16	-0,19	-0,50	-1170	1,3	94	2,2	85
	(0.10)	*(0.11)*	*(0.08)*	*(0,12)*	*(0,19)*	*(0,19)*	*(0,08)*	*(190)*	*(0,7)*	*(4)*	*(0,4)*	*(51)*
ALL	-0.94	-0.90	-0.86	-0,94	-0,13	-0,26	-0,54	-1240	1,2	97	1,9	48
	(0.08)	*(0.09)*	*(0.09)*	*(0,08)*	*(0,15)*	*(0,27)*	*(0,08)*	*(210)*	*(0,7)*	*(3)*	*(0,3)*	*(39)*

TML = Total mass loss, TRB = Total reserve in bases (Ca, K, Na, Mg), SA = Silicon-aluminium ratio, CIA = Chemical index of alteration.

Table 4. Overview of the results of the one-way ANOVA (Holm-Sidak method, $p < 0.05$) for vegetation type and topographic position. When data were drawn from non-normal populations or did not have equal variances, we performed a Kruskal-Wallis One-Way Analysis of Variance on Ranks (Dunn´s method, $p < 0.05$)

	Effect of topography	Effect of vegetation			
			Posthoc comparisons ($p < 0.05$)		
Parameter	*p-value*	*p-value*	CU vs PR	CU vs FR	PR vs FR
τ Ca (-)	0.116	0.001	Y	Y	N
τ K (-)	0.090	0.032	N	Y	N
τ Mg (-)	0.057	0.357	-	-	-
τ Na (-)	0.095	0.003	Y	Y	N
τ Si (-)	0.067	0.025	N	Y	N
τ Al (-)	0.467	0.105	-	-	-
τ Fe (-)	0.398	0.001	N	Y	Y
Strain (-)	0.856	0.392	-	-	-
TML (kg m^{-2})	0.082	0.025	N	Y	Y
TRB (cmol.kg^{-1})	0.216	0.009	Y	N	N
SA (-)	0.774	0.053	-	-	-
CIA (-)	0.247	0.001	Y	Y	N
OC (%)	0.809	0.129	-	-	-
BD (g.cm^{-3})	0.651	0.568	-	-	-
pH (-)	0.508	<0.001	Y	Y	N
ECEC (cmol(+) kg^{-1})	0.369	0.179	-	-	-
BS (%)	0.751	<0.001	Y	Y	N
Al^{3+} (cmol(+) kg^{-1})	0.724	<0.001	Y	Y	N
Al_o (g kg^{-1})	0.968	0.021	Y	Y	N
Al_p (g kg^{-1})	0.897	0.006	Y	Y	N
SD (cm)	0.499	0.007	Y	N	N

TML = Total mass loss, TRB = Total reserve in bases (Ca, K, Na, Mg), SA = Silicon-aluminium ratio, CIA = Chemical index of alteration, OC = Organic carbon content, BD = Bulk density, pH = soil pH, ECEC = Effective cation exchange capacity, BS = Base saturation, Al^{3+} = Exchangeable aluminum, Al_p = Pyrophosphate-extractable aluminum, Al_o = Oxalate-extractable aluminum and SD = Soil depth to C horizon.

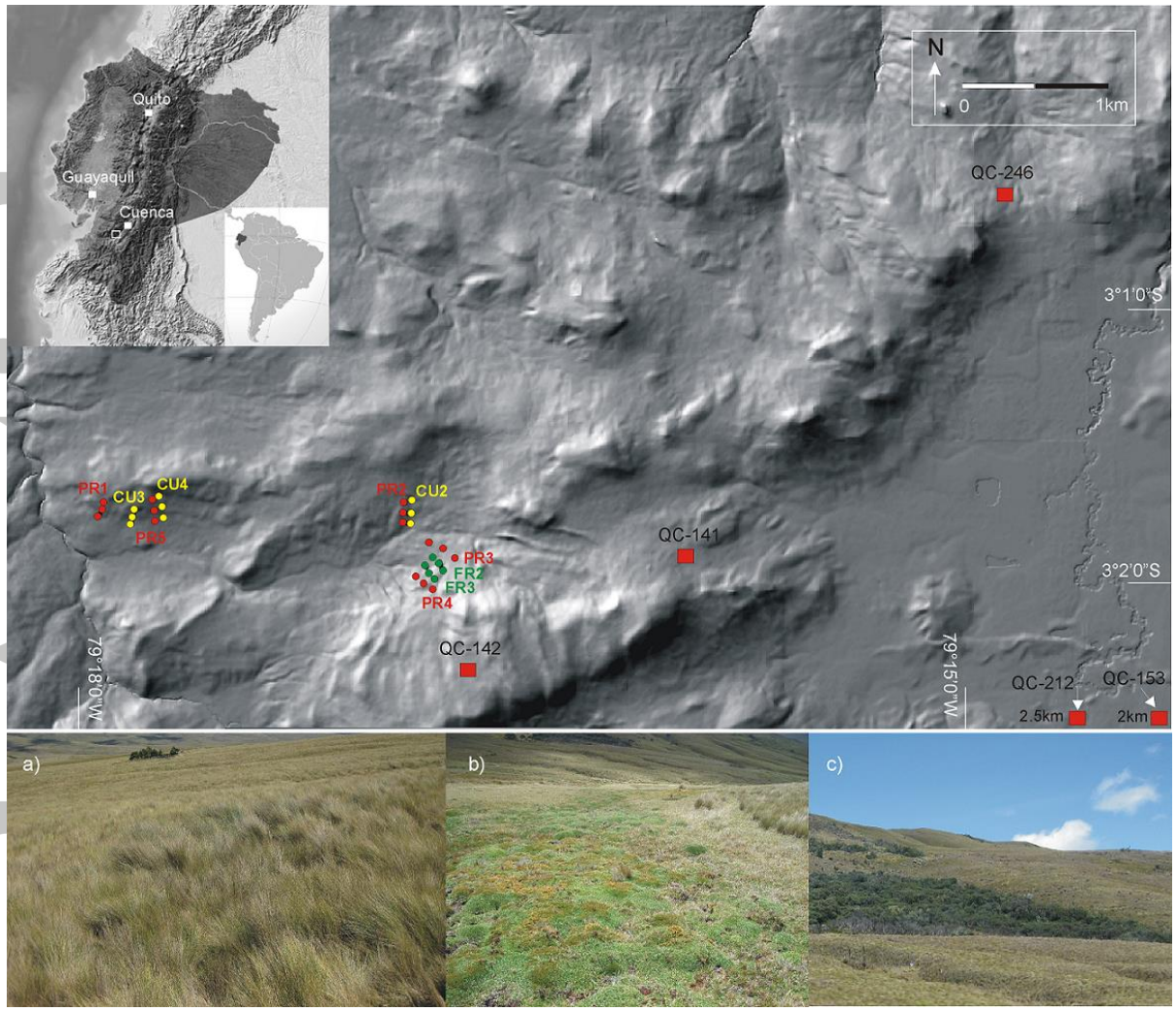

Figure 1. Topographic map of the study site, with location of 10 toposequences. The thirty dots show the location of the soil pits (dots are coloured by vegetation type with forest: green; tussock grasses: red; and cushion forming plants: yellow), and the five red squares the location of the rock samples published in Beate et al. (2001). The inset on the upper left shows the location of the study area in the Ecuadorian Andes. The pictures illustrate the vegetation types, with a) tussock grasses, b) cushion forming plants, and c) *Polylepis* forest.

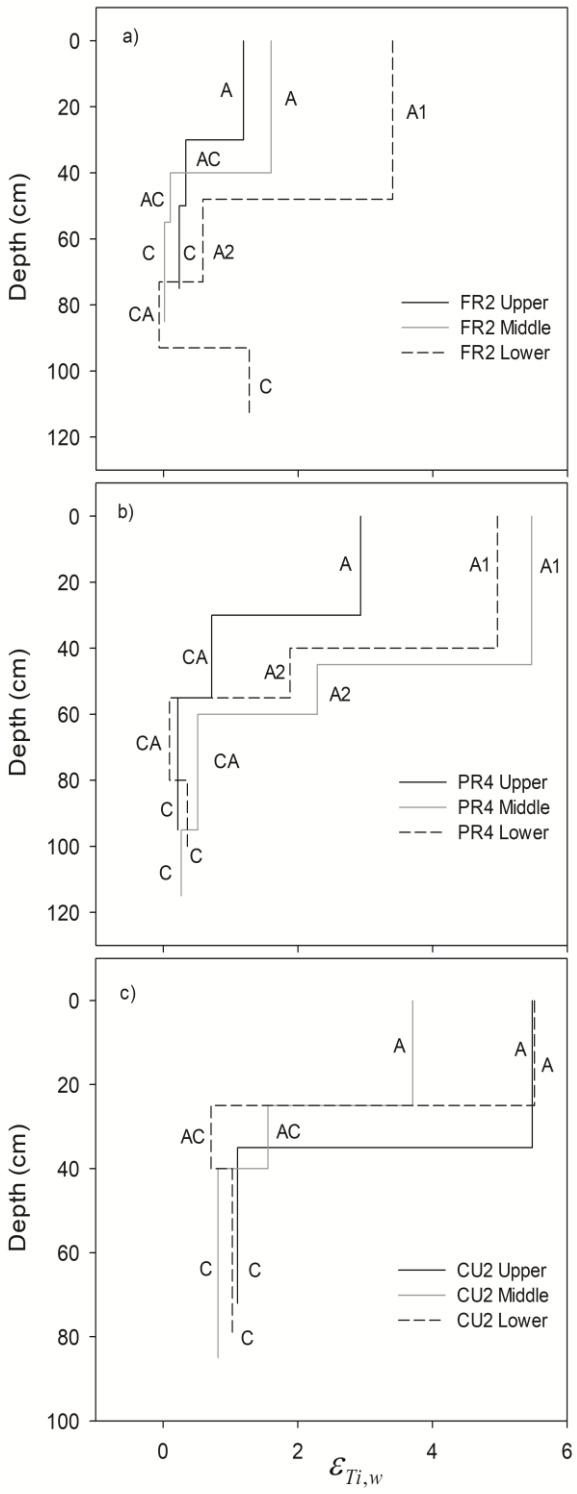

Figure 2. Volumetric strain as a function of soil depth, vegetation type and topographic position. The upper panel shows the variation in strain along a toposequence in native forests (FR2), the middle one for páramo grasslands (PR4) and the lower one for cushion plants (CU2).

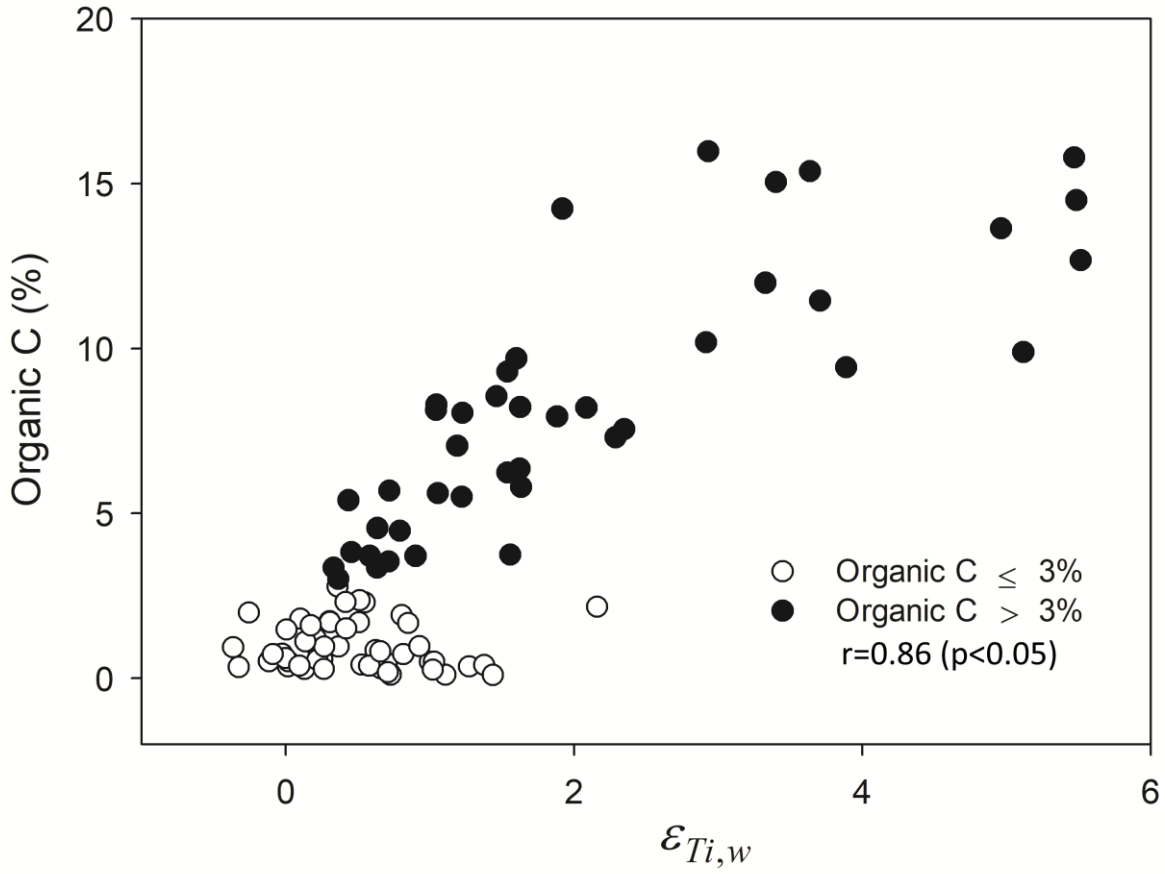

Figure 3. Soil organic C content plotted as a function of volumic deformation of the soil A horizons. For soil A horizons having a SOC above 3%, there is a positive relationship (Spearman r=0.86, p<0.05) between the SOC content and the amount of volumetric expansion.

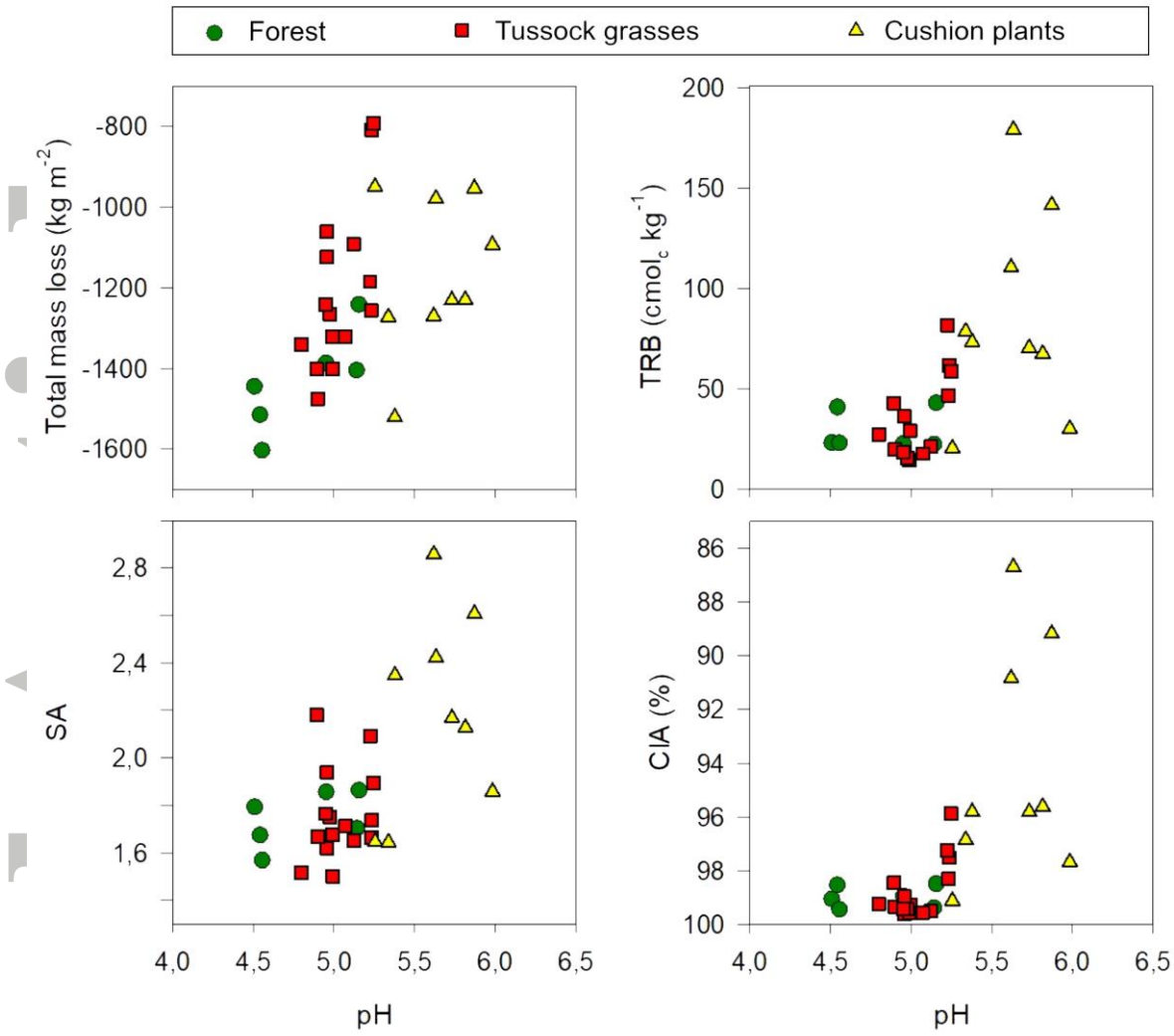

Figure 4. Relationship between soil pH_{H20} and soil chemical weathering extent as measured by total mass losses, chemical index of alteration, silicon-aluminium ratio and total reserve in bases for the 30 soil profiles.

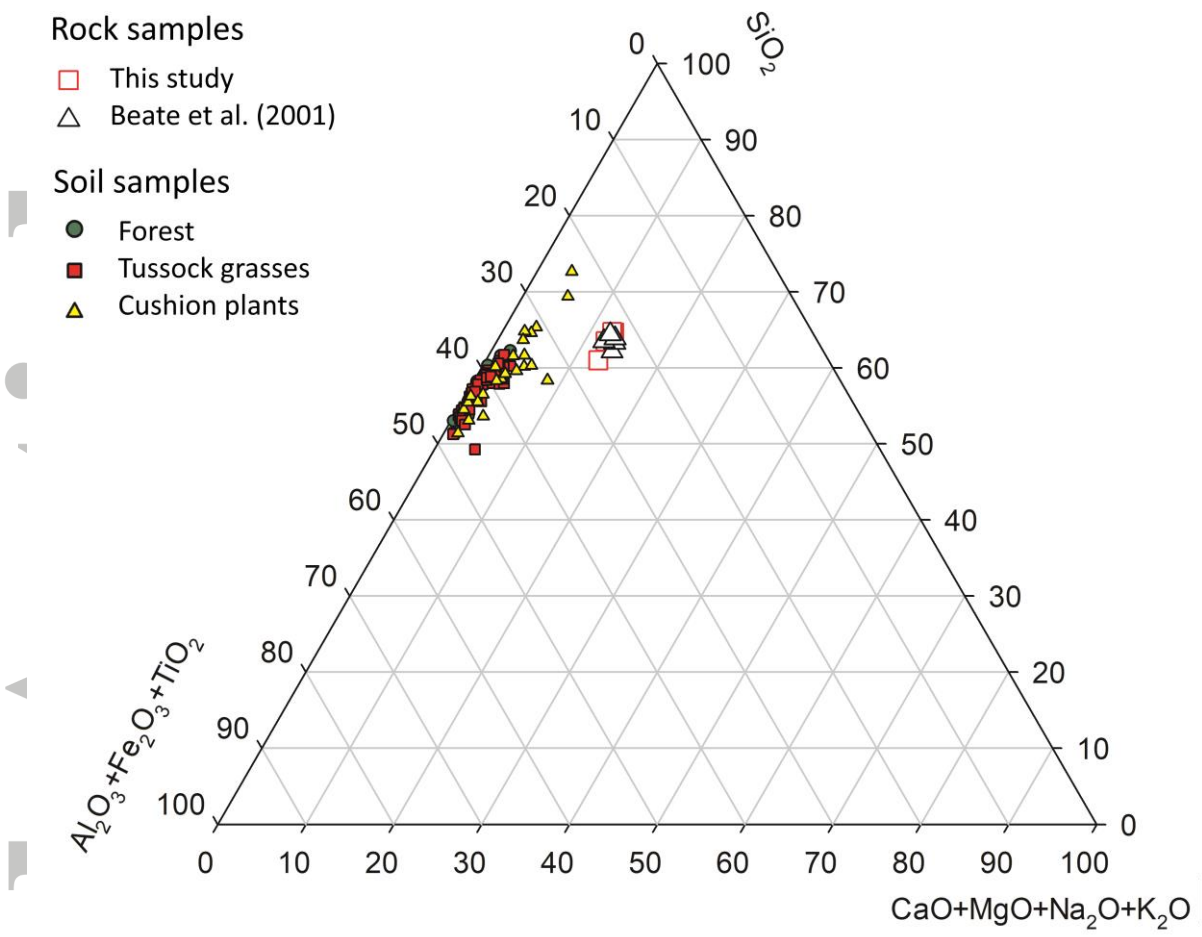

Figure 5. Ternary diagram showing the elemental geochemistry of the bedrock and soil samples. The nine rock samples are colour coded, with samples from our study sites in red rectangles, and samples from Beate et al. (2001) in black triangles. The ninety-five soil samples are colour coded according to vegetation type, with forest sites (FR) in green, tussock grasses (PR) in red, and cushion forming plants (CU) in yellow.

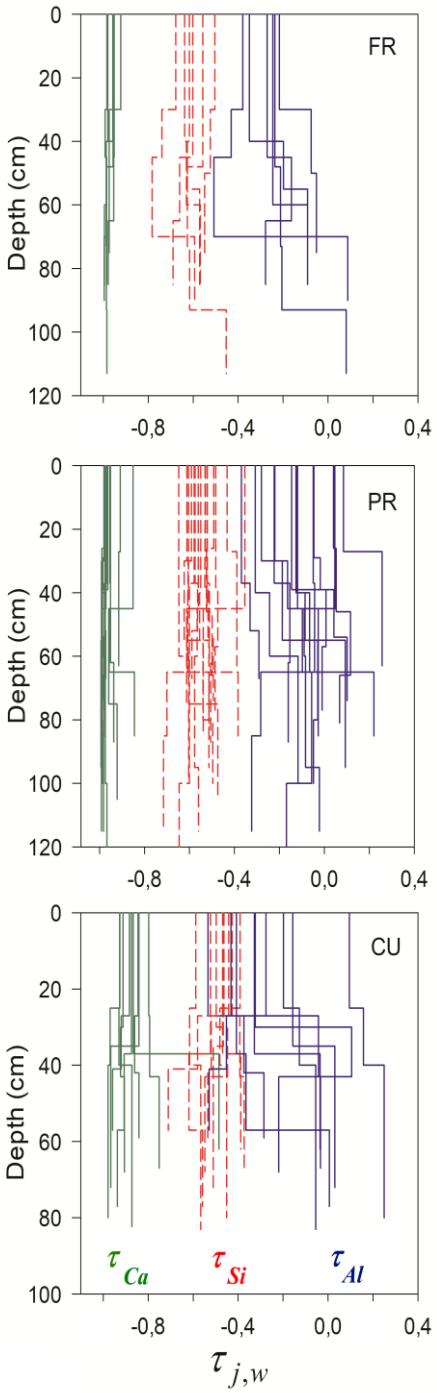

Figure 6. Depth distribution of mass transfer coefficients (τ_{Ca} in green, τ_{Si} in red, τ_{Al} in blue) of all soil profiles per vegetation type, with PR = tussock grasses, FR = *Polylepis* forests, and CU = cushion forming plants.

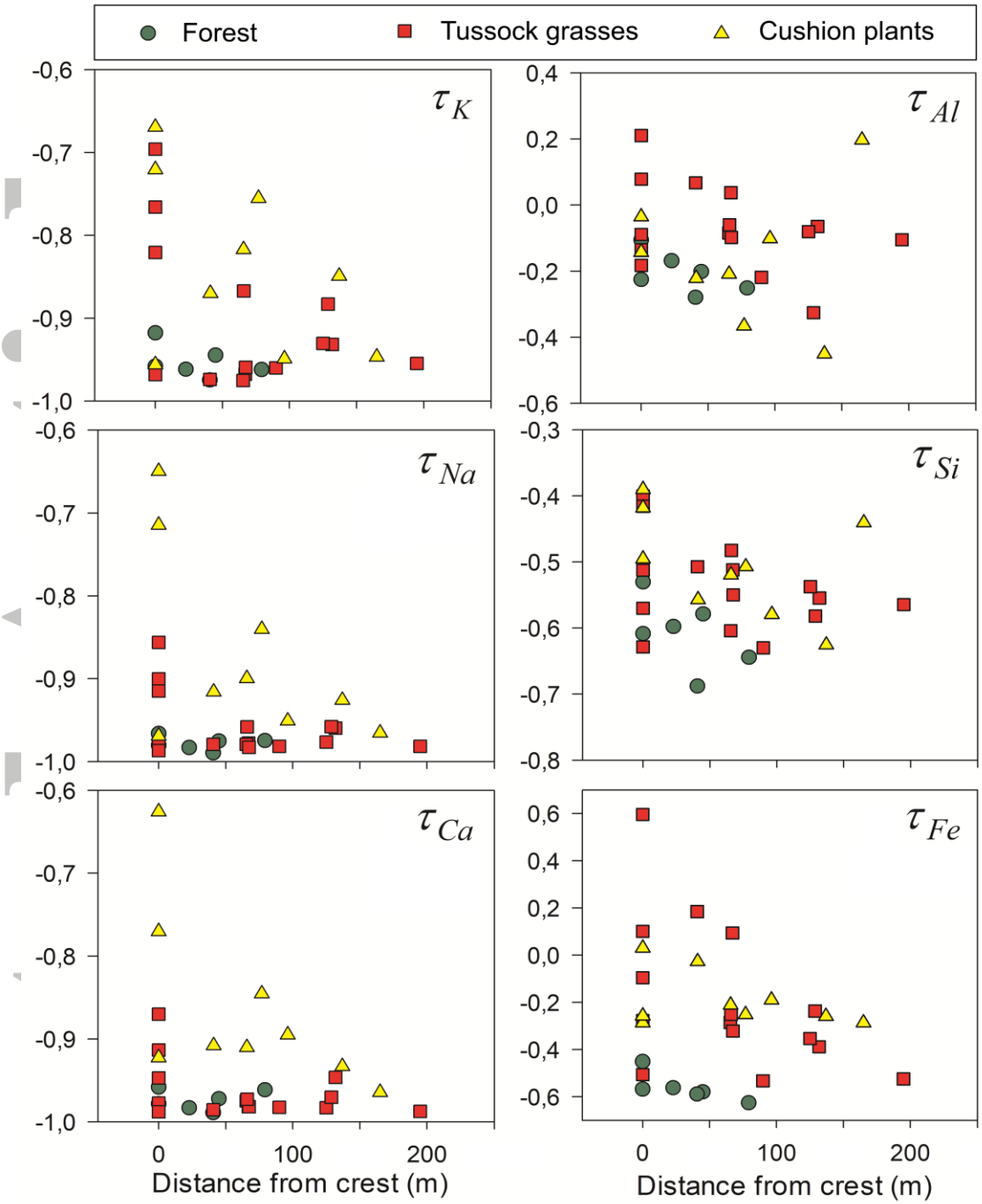

Figure 7. Depth-weighted mass transfer coefficients of the major base cations (K, Na, Ca), and metal cations (Al, Si, Fe) as a function of their topographic position, here measured as the distance from the crest. The data from the thirty soil profiles are colour coded according to vegetation type, with forest sites (FR) in green, tussock grasses (PR) in red, and cushion forming plants (CU) in yellow.

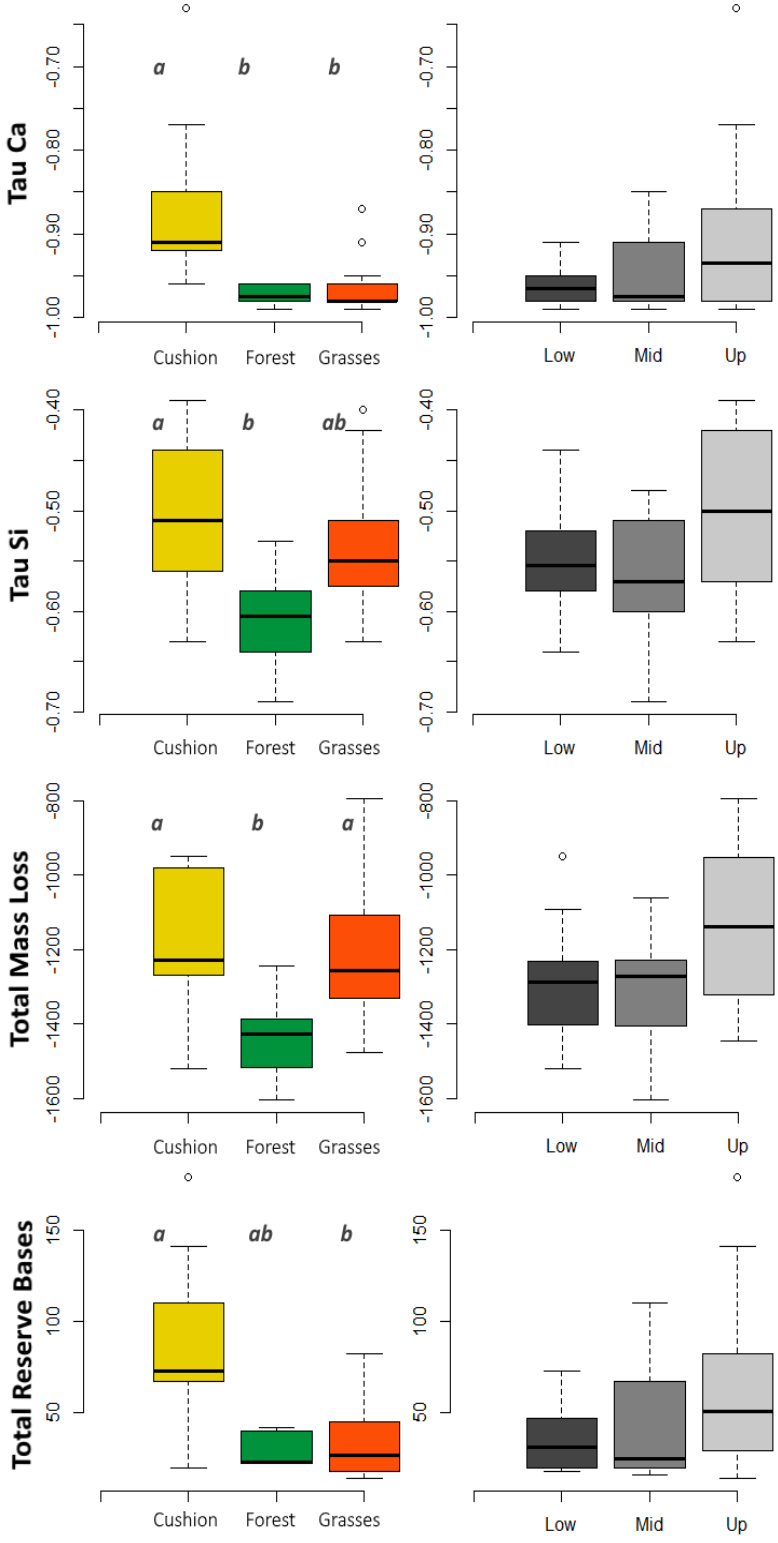

Figure 8. Boxplots illustrating the differences in τ_{Ca}, τ_{Si}, total mass loss (kg m^{-2}), and total reserve in bases ($cmol_c$ kg^{-1}) between the three vegetation types (left panels) and three topographic positions (right panels). When the one-way analysis of variance test was significant ($p < 0.05$), the results of the posthoc comparison test are shown. Boxplots with different letter differ significantly.

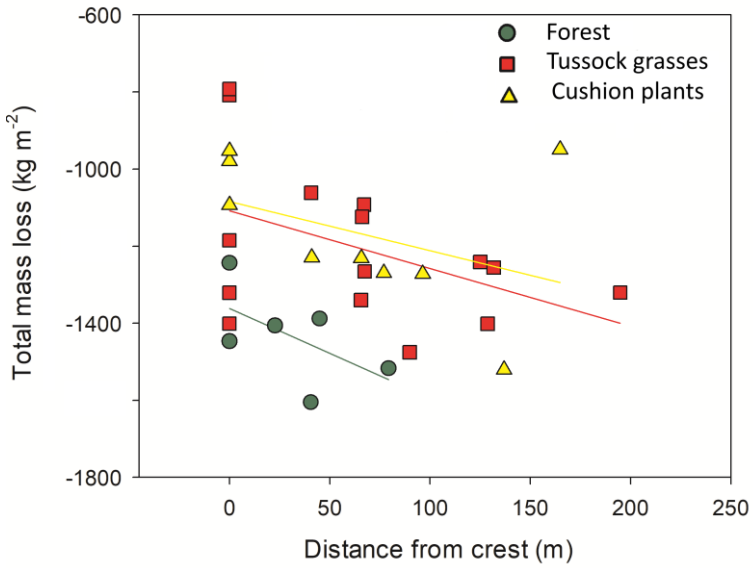

Figure 9. Total mass losses by chemical weathering of the 30 soil profiles as a function of their topographic position, here measured as the distance from the crest. Each point is a depth-weighted average of the soil profile data to a standard depth of 1 m. The data from the thirty soil profiles are colour coded according to vegetation type, with forest sites (FR) in green, tussock grasses (PR) in red, and cushion forming plants (CU) in yellow.